DARK ENERGY WITH AN ANISOTROPIC EQUATION OF STATE

Eunseong Lee
Master's thesis
Institute of Theoretical Astrophysics
University of Oslo
Norway

3rd June, 2013

Abstract

We investigate cosmologies where the accelerated expansion of the universe is driven by a fluid with an anisotropic equation of state. If dark energy equation of state is anisotropic, the expansion rate of the universe becomes direction dependent at late times. We show that such models are cosmologically viable. We model such scenarios within axisymmetric limit, described by the Bianchi I, Bianchi III and Kantowsk-Sachs geometries. A skewness parameter is introduced to quantify the deviation of pressure from isotropy. We study the dynamics of the background expansion in these models. The fixed points are found with the aim of uncovering their stability and employing them to device possibly realistic cosmological models.

Acknowledgments

I would like to thank my great supervisor David Mota and Tomi Koivisto who came up with the idea for this thesis. I greatly thank them for always being amazingly supportive and having confidence in me. I could not have completed it without their constant encouragement. Special thanks to Tomi Koivisto for patiently answering all my questions and investing great deal of time to complete this thesis. Also I would like to thank my fellow students at the Institute of Theoretical Astrophysics, especially Max Grönke for always helping me so pleasantly and reading through my theis as well, and Elisabeth Jordahl for sharing most of time in this master program and making it much more enjoyable. I wish to thank my family in Korea for financial and moral support from far away. Finally, I would like to thank specially to Stephen Wolfram.

Introduction

Observational data shows that a homogeneous and isotropic universe is a fairly good approximation to the real universe we live in (Partridge and Wilkinson 1967). The large-scale structure of the universe also implies that it is possibly the most symmetrical system (Peebles 1980). However recent observations in the cosmic microwave background temperature anisotropies suggest the need of reconsideration for some basic assumptions (Copi et al. 2010).

The statistical analysis of the WMAP data show the lack of large-scale power in CMB (Hinshaw et al. 2007). Clear asymmetries between pairs of hemispheres have been observed. It turned out that the northern galactic and ecliptic hemispheres have much fewer large-scale fluctuations than the simulated maps (Eriksen et al. 2004). The anomalous lack of power at the large scales in CMB maps seems to be due to missing angular correlations of quadrupole-like signiture (Bernui et al. 2006). An unexpected property in the brightness distribution of the quadrupole and octupole moments, which is known as the Axis of Evil, is also recognized (Land and Magueijo, 2007). It is also shown that the Axis of Evil as an axisymmetric effect is incompatible with the observed microwave sky at the largest angular scales (Rakić and Schwarz 2007). Whether these observed large-scale anomalies are caused by the cosmological origin or the statistical consequence is still debatable (Copi et al. 2006; Magueijo and Sorkin 2007; Komatsu et al. 2011).

There have been various possible cosmological causes to explain these anomalous features. For example anisotropy can be created by introducing a preferred axis. It can be classified into the different models depending on when this isotropy breaking happens. If it occurs at an early time, its statistical anisotropy may be imprinted in the primordial perturbations (Armendáriz-Picón 2006). It is shown that CMB radiation may become statistically anisotropic by introducing spacetime noncommutativity which causes nontrivial contributions to the CMB fluctuations (Akofor et al. 2008). The possibility that rotational invariance can be broken during inflation when the primordial density fluctuations were created has been studied (Ackerman et al. 2007). Therefore these primordial perturbations depending on their directionality are left by isotropization (Gumrukcuoglu et al. 2006). Parity violation in

the early universe is also suggested to explain the observed loss in power and the alignment at a preferred axis in the low mulitpole moments (Alexander 2008).

If CMB is distorted at late times, the originally isotropic CMB fluctuation can be broken spontaneously due to the long wavelength fluctuations in a mediating field (Gordon et al. 2005). In these cases, anisotropic fluctuations should appear at the smallest multipoles that correspond to the wavelengths entering inside the horizon. Fortunately it occurs exactly when dark energy begins to dominate and it might be an answer to one of coincidence problems of why the cosmic acceleration began when it did (Dalal et al. 2001). Dark energy in a form of vector field can be related to the statistical anisotropy (Armendáriz-Picón 2004; Böhmer and Harko 2007; Koivisto and Mota 2008). Shear viscous fluids can be associated with dark energy to explain statistical anisotropy as well (Koivisto and Mota 2006). Modified gravity theories (Clifton et al. 2005; Koivisto 2006; Tsujikawa 2010) predict that dark energy would have anisotropic stresses at least at the perturvative level, if dark energy is not the cosmological constant. It can be used to distinguish scalar field theories in which the field is strongly coupled to the perfect fluid matter (Koivisto 2005; Mota and Shaw 2007). These shear stresses in perturbation can be constrained by the viscosity properties of fluids (Capozziello et al. 2006; Mota et al. 2007). When the perturbative anisotropic stress is limited to a large scale, it can only be seen on amplitudes of the small multipoles of the CMB which makes it possible to escape detection. Fortunately there are suggested models that dark energy can form small wavelength perturbations when the Jeans scale of the dark energy is small enough. In that case it can be detected by using weak lensing experiments (Schimd et al. 2005).

In this work, we continue a previous study about the origins and implications of an anisotropic acceleration in a flat universe (Koivisto and Mota 2008). Here the system is constructed in coordinate system and study is extended to a curved space-time, that is $k = 0$, as well. We study exact anisotropic but homogeneous solutions of the cosmological equations. For a flat geometry, Bianchi I model is simple enough to allow analytical computations and it shows the basic effect even in more complicated anisotropic models by featuring direction-dependent expansion rates. The constraints on the Bianchi models imply that the universe may initially be anisotropic but isotropize later. If a solution does not isotropize, anisotropic matter sources would be needed and it should dilute slower than dust or radiation. The existence of such cosmological sources has not been known. However it is obvious that our universe is dominated by an unexplained negative pressure, we would like to ask whether this pressure could be anisotropic as well. This would connect the present acceleration of the universe with the possible anomalous features in the largest angular scales, otherwise the coincidence of the scales would seem to require additional fine tuning. This opens a window to study the nature of dark energy by constraining its possible anisotropy.

Contents

Chapter 1

Preliminaries

In this chapter, the theoretical basics will be introduced. First, we will discuss briefly the theory of general relativity. Secondly, we will review the cosmological concepts.

1.1 The theory of general relativity

In general relativity gravity is considered as a geometric property of spacetime not a force. Applying the Einstein equations to a given metric gives the relation between the parameters in the metric and the contents in the universe. This is why the theory of general relativity has been a framework to construct most of cosmology models. In order to make use of it we need to understand a metric first, which is an essential concept in general relativity.

1.1.1 The metric

In most astronomical work, it is crucial to be able to compute the distance between two events in a four-dimensional spacetime. Simply calculating the physical distance between two points in a three-dimensional flat space is not difficult. However in an expanding (or contracting) universe, it becomes much less simple. One needs to introduce a scale factor connecting the coordinate distance with the physical distance. This is because it makes the metric an important mathematical tool for predicting the universe we live in. From the components of the metric we can introduce the infinitesimal interval or, the line element ds

$$ds^2 = g_{\mu\nu} dx^\mu dx^\nu \tag{1.1}$$

where dx^μ is an infinitesimal coordinate displacement between two spacetime events in the direction of the coordinate x^μ. The indices μ and ν range from 0 to 3 where the first one is a time-like coordinate, $dx^0 = dt$ and the last three are spatial coordinates. The metric $g_{\mu\nu}$ is necessarily symmetric, so it has four diagonal and six non-diagonal elements in four-dimensional spacetime. The most general line element of a homogeneous and isotropic universe in spherical polar coordinates (Carroll 2004) is

$$ds^2 = -dt^2 + a^2(t)\left[\frac{dr^2}{1-kr^2} + r^2(d\theta^2 + \sin^2\theta d\phi^2)\right] \tag{1.2}$$

where t is the proper time as measured by a comoving observer and $a(t)$ is a scale factor which is proportional to the physical distance. Its present value is usually set to one for convenience. One notes that the comoving distance remains constant as the universe expands. On the other hand, the physical distance increases with time. A curvature parameter k is included in the metric. $k > 0$ represents a positively curved space (closed, sphere when $k = +1$), $k = 0$ represents a flat space, and $k < 0$ represents a negatively curved space (open, hyperboloid when $k = -1$). These are all local concepts. This metric is called the Robertson-Walker (RW) metric.

1.1.2 The Einstein equations

The Einstein equations are

$$G_{\mu\nu} = 8\pi G T_{\mu\nu} \tag{1.3}$$

where $G_{\mu\nu}$ is the Einstein tensor, G is Newton's gravitational constant, and $T_{\mu\nu}$ is the energy-momentum tensor describing the constituents of the universe. Therefore the left-hand side of (1.3) is a function of the metric and the right-hand side is a function of the energy of relativistic mass (Misner et al. 1973). The time-time component of energy-momentum tensor $T_{\mu\nu}$ often represents the density of relativistic mass and the time-space or space-time components mean linear momentum density. When it comes to the space-space components, the diagonal components represents normal stress which can be interpreted as pressure when it is independent of direction and the remaining components mean shear stress. The Einstein tensor $G_{\mu\nu}$ is expressed

$$G_{\mu\nu} \equiv R_{\mu\nu} - \frac{1}{2} g_{\mu\nu}\mathcal{R} \tag{1.4}$$

where $R_{\mu\nu}$ is the Ricci tensor and $\mathcal{R}$ is the Ricci scalar defined by the contraction of the Ricci tensor ($\mathcal{R} \equiv g^{\mu\nu}R_{\mu\nu}$). The Ricci tensor $R_{\mu\nu}$ can be written in terms of the Christoffel symbol,

$$R_{\mu\nu} = \Gamma^\alpha{}_{\mu\nu,\alpha} - \Gamma^\alpha{}_{\mu\alpha,\nu} + \Gamma^\alpha{}_{\beta\alpha}\Gamma^\beta{}_{\mu\nu} - \Gamma^\alpha{}_{\beta\nu}\Gamma^\beta{}_{\mu\alpha} \tag{1.5}$$

where commas denote derivatives with respect to x, for example

$$\Gamma^{\alpha}{}_{\mu\nu,\alpha} = \frac{\partial \Gamma^{\alpha}{}_{\mu\nu}}{\partial x^{\alpha}} \tag{1.6}$$

Here the Christoffel symbol is

$$\Gamma^{\mu}{}_{\alpha\beta} = \frac{g^{\mu\nu}}{2}\left[\frac{\partial g_{\alpha\nu}}{\partial x^{\beta}} + \frac{\partial g_{\beta\nu}}{\partial x^{\alpha}} - \frac{\partial g_{\alpha\beta}}{\partial x^{\nu}}\right] \tag{1.7}$$

The Christoffel symbol arises when we take the covariant derivate of a metric tensor. In general relativity, Christoffel symbol plays the role of the gravitational force field. Note that it is not a tensor (Kusse and Westwig 2010). Then geodesic equation in general also can be written in terms of the Christoffel symbol

$$\frac{d^2x^{\mu}}{d\lambda^2} = -\Gamma^{\mu}{}_{\alpha\beta}\frac{dx^{\alpha}}{d\lambda}\frac{dx^{\beta}}{d\lambda} \tag{1.8}$$

where λ is a parameter which increases along the particle's path. The geodesic is the notion of shortest or straight line in spacetime and defined as the path followed by a particle in the absence of any forces. In a Cartesian coordinate system, the Christoffel symbol vanishes and the geodesic equation becomes zero. However generally they do not vanish and their existence describes geodesics in nontrivial coordinate systems (Dodelson 2003).

1.2 Homogeneous and isotropic cosmology

1.2.1 Maximally symmetric universe

Copernican principle means that the universe is almost exactly the same everywhere, in other words no point in the universe is special. It has turned out, we are not a privileged observer. Therefore the earth is neither in the center of the universe, nor is it in a spatially favoured position. The copernican principle is connected to these two mathematical properties :isotropy and homogeneity. These two concepts appear to be similar, however they bring quite a different description to the universe as a whole.

Isotropy is having the same property in all directions(Freedman and Kaufmann 2002). Same observational evidence is available by looking in any direction in the universe. Isotropy applies at some specific point. The space looks the same no matter in what direction an observer looks.

Homogeneity is having the same property in one region as in every other region. Same observational evidence is available to observers at different locations in the

universe. It is obviously false in local scale though, it works statistically in scales of the millions light-years. Then the average density of matter is almost same thorough the whole universe, so the universe is smooth in density on large scales.

There is no necessary relationship between isotropy and homogeneity. At least the isotropy for all observers implies the homogeneity for all observers (Peacock 1999). It is possible to build homogeneous but anisotropic universes, but the reverse is not possible (Barrow and Matzner 1977).

Cosmological principle is derived from the copernican principle but it cannot be proved in a mathematical sense. It is supported by the empirical grounds, for example observations of the uniform temperature distribution of the cosmic microwave background. In other words, when it comes to cosmological principle, it can be understood that on large scales the universe is both homogeneous and isotropic (Hawking and Ellis 1973).

The great advantage of having homogeneity and isotropy is that it is assumed that the universe is fairly spatially symmetric. Isotropy can be considered as a rotational invariance and homogeneity as a translational invariance. This maximally symmetric universe can be a gound state of general relativity and is considered the standard model of cosmology today.

1.2.2 The Friedmann equations

The RW metric is defined for scale factor (1.2). Plugging it into Einstein's equations gives the Friedmann equations connecting the energy-momentum of the universe with the scale factor. In the case of a perfect isotropic fluid, the energy-momentum tensor becomes

$$T^{\mu}{}_{\nu} = \text{diag}\ (-\rho,\ p,\ p,\ p) \tag{1.9}$$

where ρ is the energy density and p is the pressure of the fluid. The trace is simply given by $T^{\mu}{}_{\mu} = -\rho + 3p$. We assume that there is no gravity and velocities are negligible. Then the energy density and pressure evolve according to the continuity equation, $\partial\rho/\partial t = 0$ and the Euler equation, $\partial p/\partial x^i = 0$. It becomes a conservation equation for the energy-momentum tensor,

$$T^{\mu}{}_{\nu;\mu} = 0 \tag{1.10}$$

since we chose a perfect isotropic fluid,

$$\frac{\partial\rho}{\partial t} + 3\frac{\dot{a}}{a}(\rho + p) = 0 \tag{1.11}$$

Defining a relationship between ρ and p which is the *equation of state* gives

$$p = \omega\rho \tag{1.12}$$

where ω is called the equation-of-state parameter which is often set to be independent of time but it is not necessary. If we restrict ourselves to sources with $\rho \geq 0$, then the energy conditions [1] will imply $\omega \leq |1|$ (Visser and Barceló 2000). Then the conservation of energy equation becomes

$$\frac{\dot{\rho}}{\rho} = -3(1+\omega)\frac{\dot{a}}{a} \tag{1.13}$$

Assuming that ω is constant and integrating it gives

$$\rho \propto a^{-3(1+\omega)} \tag{1.14}$$

It can be applied to obtain information about the scaling of cosmological fluids. Matter is collisionless and nonrelativisitc particles which are known as dust. It has effectively zero pressure. When the universe is *matter-dominated* the energy density in matter scales

$$p_{\rm m} = 0 \quad \longrightarrow \quad \rho_{\rm m} \propto a^{-3} \tag{1.15}$$

Radiation is either actual photons or relativistic particles. When the universe is *radiation-dominated* the energy density in radiation scales

$$p_{\rm r} = \frac{1}{3}\rho_r \quad \longrightarrow \quad \rho_{\rm r} \propto a^{-4} \tag{1.16}$$

accounting for the additional loss in energy as photons redshift due to the expansion. Vacuum energy can be considered as a form of perfect fluid. If a vacuum energy is nonzero the universe can be dominated by vacuum energy at late times, since the energy density for matter and radiation die out as the universe expands . When the universe is *vacuum-dominated* the energy density scales

$$p_\Lambda = -\rho_\Lambda \quad \longrightarrow \quad \rho_\Lambda = \text{constant} \tag{1.17}$$

Einstein's equation from (1.3) and (1.4) can be written in the form

$$R_{\mu\nu} - \frac{1}{2}g_{\mu\nu}\mathcal{R} = 8\pi G T_{\mu\nu} \tag{1.18}$$

The Ricci tensor and Ricci scalar can be calculated by using the Christoffel symbol (1.7) in Robertson-Walker metric (1.2).

$$\begin{aligned} R_{00} &= -3\frac{\ddot{a}}{a} \\ R_{11} &= \frac{\ddot{a}a + 2\dot{a}^2 + 2k}{1-kr^2} \\ R_{22} &= r^2(\ddot{a}a + 2\dot{a}^2 + 2k) \\ R_{33} &= r^2(\ddot{a}a + 2\dot{a}^2 + 2k)\sin^2\theta \\ \mathcal{R} &= 6\left[\frac{\ddot{a}}{a} + \left(\frac{\dot{a}}{a}\right)^2 + \frac{k}{a^2}\right] \end{aligned} \tag{1.19}$$

[1] The Null Dominant Energy Condition allows for a vacuum energy of either positive or negative sign but otherwise requires matter that cannot destabilized the vacuum (Carroll et al. 2003).

Applying (1.19) to the equation (1.18) and rearranging, we can find

$$\left(\frac{\dot{a}}{a}\right)^2 + \frac{k}{a^2} = \frac{8\pi G}{3}\rho \tag{1.20}$$

and

$$\frac{\ddot{a}}{a} = -\frac{4\pi G}{3}(\rho + 3p) \tag{1.21}$$

The two *Friedmann equations* are finally derived from the Einstein equations. The RW metric (1.2) corresponding to these Friedmann equations defines Friedmann-Robertson-Walker universes (Carroll 2004). The *density parameter* is also a useful cosmological quantity, so we define

$$\Omega \equiv \frac{\rho}{\rho_{\text{crit}}} \tag{1.22}$$

where the *critical density* is defined by

$$\rho_{\text{crit}} \equiv \frac{3H^2}{8\pi G} \tag{1.23}$$

where $H \equiv \dot{a}/a$ is the Hubble parameter. From the first Friedmann equation (1.20)

$$\Omega - 1 = \frac{k}{H^2 a^2} \tag{1.24}$$

The sign of curvature k depends on the density parameter Ω. The recent observations of the cosmic microwave background anisotropy shows that Ω has to be very close to unity. Here we can set one more important cosmological parameter. From (1.24) the curvature parameter can be defined

$$\Omega_{\text{k}} \equiv -\frac{k}{H^2 a^2} \tag{1.25}$$

with corresponding energy density term

$$\rho_{\text{k}} \equiv -\frac{3k}{8\pi G a^2} \quad \longrightarrow \quad \rho_{\text{k}} \propto a^{-2} \tag{1.26}$$

This term does not mean an energy density though, still it is convenient to express the contribution of spatial curvature as an energy density parameter. So far the description of energy density ρ for different species with its equation of state $p = \omega\rho$ and the spatial curvature k are found. Now we are ready to solve the Friedmann equation (1.20) to obtain the evolution of the scale factor $a(t)$. The Friedmann equation is simply a first-order differential equation which can be easily integrated. Firstly the Friedmann equation (1.20) may be written as follows

$$H^2 = \frac{8\pi G}{3}\sum_i \rho_i \tag{1.27}$$

where ρ_i is the energy density of different species i including the contribution of spatial curvature. H^2 is proportional to $\sum_i \rho_i$. If all the energy density components are positive, the universe will keep expanding. There will be no such transition from expansion to contraction, which requires H to be zero. Dividing both sides by H^2 we find

$$1 = \sum_i \Omega_i \tag{1.28}$$

Note that the right-hand side is not the total energy density parameter Ω. It only covers the actual energy density contributions not the curvature so that $\Omega_{\rm k} = 1 - \Omega$. Even though the real universe seems to be the combination of matter, radiation and vacuum energy, it is still useful to have solutions to the Friedmann equation for a single energy source. Since different sources evolve at different rates, there will be a period which is clearly dominated by one kind of source. When one single species dominates the energy density the scale factor a can be simply expressed in terms of time t. For example we consider a flat matter-dominated case, $\Omega = \Omega_{\rm m} = 1$, which is known as the *Einstein-de Sitter universe*. In this universe, the scale factor evolves as $a \propto t^{2/3}$. If a universe is flat and radiation-dominated, evolves as $a \propto t^{1/2}$. There can be a universe without matter and radiation, but spatially flat due to the vacuum energy. The universe with a positive cosmological constant is called the *de Sitter universe* and evolves as $a \propto e^{Ht}$. The completely empty universe can be an interesting special case. No energy density but only with spatial curvature, $\Omega = \Omega_{\rm k} = 1$. From (1.25) we see that a universe will expand linearly, $a \propto t$. This is known as *Milne universe*. Taking the time derivate of the Hubble parameter H, we obtain

$$\dot{H} = \frac{\ddot{a}}{a} - \left(\frac{\dot{a}}{a}\right)^2 \tag{1.29}$$

and plugging it into the two Friedmann equations (1.20) and (1.21) to find

$$\dot{H} = -4\pi G \sum_i (1 + \omega_i)\rho_i \tag{1.30}$$

In the limit of $|\omega_i| \leq 1$, if all the energy density components are positive, $\dot{H}$ will never be positive which means the universe keeps expanding, but the rate of expansion decreases gradually. There can be a case that $\ddot{a}$ is positive but $\dot{H}$ is negative, it can be shown easily from (1.29). In spite of the decreasing expansion rate measured by the Hubble parameter H, the scale factor a can be accelerating. The derivative of the scale factor and the Hubble parameter are explaining two different situations. One would be how the fixed source moves away from us with time. Then the answer would be given by the change in the scale factor. The other would be about two sources at fixed initial distance and how much these two have separated sometime after. Then the answer would be given by the Hubble parameter. These two are conceptually different, however can be considered in the sense of explaining acceleration or deceleration, when acceleration is defined as $\ddot{a} > 0$.

1.2.3 Redshift and distances

The cosmic redshift

In mechanics, redshift is considered as a result of the Doppler effect, a change of a wavelength for an observer moving relative to its source. As a result, the received wavelength is shorter when its approach and is longer when its recession compared to the emitted wavelength. However the cosmic redshift is more specialized in a certain sense, since it can be interpreted as a consequence of the expansion of the universe. In general, it happens when a sufficiently distant source is moving away from an observer. Also gravitational redshifts occur when a light source escapes from the gravitational field. We consider the electromagnetic waves coming towards us at the origin. The first wave is emitted at a cosmic time t_e and the second wave is emitted infinitesimally later at time $t_e + \delta t_e$. Then we observe them at t_o and $t_o + \delta t_o$. Since the light follows a path defined by $ds^2 = 0$ and travels along a line of $\theta = \phi =$ constant, the RW line element becomes [2]

$$0 = dt^2 - a^2(t)\frac{dr^2}{1-kr^2} \quad \longrightarrow \quad \frac{dt}{a(t)} = -\frac{dr}{\sqrt{1-kr^2}} \tag{1.31}$$

Integrating it for the first and second wave from the emission to the observation time which should be the same for the both case

$$\int_{t_e}^{t_o} \frac{dt}{a(t)} = \int_{t_e+\delta t_e}^{t_o+\delta t_o} \frac{dt}{a(t)} \tag{1.32}$$

Rearranging

$$\int_{t_e}^{t_e+\delta t_e} \frac{dt}{a(t)} = \int_{t_o}^{t_o+\delta t_o} \frac{dt}{a(t)} \quad \longrightarrow \quad \frac{\delta t_e}{a(t_e)} = \frac{\delta t_o}{a(t_o)} \tag{1.33}$$

It implies $\delta t_e < \delta t_o$ which means that the expansion of universe stretches the wavelength of the photons. Then we can get the relation

$$\frac{\lambda_o}{\lambda_e} = \frac{a(t_o)}{a(t_e)} \equiv 1 + z \tag{1.34}$$

where $\delta t_e = \lambda_e$ and $\delta t_o = \lambda_o$. The cosmic redshift is parametrized by z and measures how much the universe has expanded between the times of emission and observation. The cosmic redshift is often referred to the redshift of an epoch, since it is observationally available quantity and determines unique cosmic time of emission.

[2] As an electromagnetic wave moves towards us at the origin, r decreases so that $dr < 0$ for $dt > 0$.

The proper distance

Measuring distance in an expanding universe is tricky. One simple way of handling this is calculating distances at a given time t as the universe is still. This is called a proper distance which is the shortest path (spatial geodesic) in space between two points at an exact time t. The scale factor $a(t)$ is fixed as well. The proper distance is denoted by $d_{\rm P}(t)$ and is given by

$$d_{\rm P}(t) = a(t) \int_0^r \frac{dr'}{\sqrt{1-kr'^2}} = a(t)\, \mathcal{S}^{-1}(r) \tag{1.35}$$

where

$$\mathcal{S}^{-1}(r) = \begin{cases} \sin^{-1} r & \text{for } k = +1 \\ r & \text{for } k = \ \ 0 \\ \sinh^{-1} r & \text{for } k = -1 \end{cases} \tag{1.36}$$

For the spatially flat universe, $k = 0$ the proper distance is $d_{\rm P}(t) = a(t)r$. This is just the comoving coordinate r, which is a constant in time, times the scale factor $a(t)$. As it is shown that the proper distance $d_{\rm P}$ is a function of time t, the relative distance between the two points increases due to the expansion. The observed relative velocity is simply

$$v = \dot{d}_{\rm P}(t) = \dot{a}\, \mathcal{S}^{-1}(r) = \frac{\dot{a}}{a}\, d_{\rm P}(t) \tag{1.37}$$

Introducing the Hubble parameter $H(t) \equiv \dot{a}/a$

$$v(t) = H(t)\, d_{\rm P}(t) \tag{1.38}$$

This is Hubble's law : the observed recession velocity is directly proportional to the distance at a given time. Since the universe does not expand at the same rate at all times, the Hubble parameter in principle is a function of time. However it is common to consider the Hubble parameter as a constant H_0 for a present time t_0.

The luminosity distance

It is clear that the universe has expanded significantly during the time the light has travelled towards us. We can obtain a distance by measuring the flux from an object of known luminosity, this is called luminosity distance $d_{\rm L}$. The observed flux F, which is an emitted energy per unit time and area, can be written as

$$F = \frac{L}{4\pi d^2} \quad \longrightarrow \quad d_{\rm L} \equiv \sqrt{\frac{L}{4\pi F}} \tag{1.39}$$

where a distance d from a source of known luminosity L, which is an emitted energy per unit time. In order to generalize this result to an expanding universe,

we consider a spherical shell with radius $a(t_o)r$ at the time of observation t_o. The wavelengths of the observed photons have stretched by a factor $a(t_o)/a(t)$ at time t_o. Then the received flux F at t_o may be written

$$F = \frac{L}{4\pi a^2(t_o) r^2} \left(\frac{a(t)}{a(t_o)} \right)^2 \tag{1.40}$$

Using the definition (1.34) and (1.39) we obtain

$$d_{\rm L} = a(t_o)\, r\, \frac{a(t_o)}{a(t)} = a(t_o)\, r\, (1+z) \tag{1.41}$$

The Cepheid variables and type Ia supernovae have been used to determine distances to very large redshift z (Macri et al. 2006; Schweizer et al. 2008).

The angular diameter distance

Another way to determine distances is to measure the angle θ with the observed diameter size D at a sufficiently large distance d. The angular diameter distance is defined

$$d_{\rm A} \equiv \frac{D}{\theta} \tag{1.42}$$

We can obtain the angular diameter distance in an expanding universe by placing the observer at the origin and a source at a radial comoving coordinate r. Then the observed diameter of the source at time t becomes $a(t)\, r\, \theta$. Therefore we find

$$d_{\rm A} = a(t) r = \frac{a(t)}{a(t_o)} a(t_o)\, r = \frac{a(t_o)\, r}{1+z} \tag{1.43}$$

The angular diameter distance is the same as the proper distance at low redshift, but decreases at very large redshift. From the definitions (1.41) and (1.43) we can find the relation between the luminosity distance and the angular diameter distance

$$\frac{d_{\rm L}}{d_{\rm A}} = (1+z)^2 \tag{1.44}$$

1.2.4 Dark energy

The recent results from Planck in Fig. 1.1 show that the total mass-energy of the universe contains 4.9% ordinary matter, 26.8% dark matter, and 68.3% dark energy. Even though dark energy is still unknown, it is the most accepted hypothesis to account for the accelerating expansion of the universe. The observation of the supernovae (Suzuki et al. 2012), the cosmic microwave background anisotropies

(Komatsu et al. 2011), and the large scale structure (Blake et al. 2011) are the indication of the existence of dark energy.

One explanation for dark energy is that it is space itself that is the so-called *cosmological constant* Λ. It is also called vacuum energy because it is an energy density of empty vacuum (Peebles and Ratra 2003). According to classical thermodynamics the cosmological constant should have a negative pressure, which means that, for example, the equation of state parameter ω in (1.12) is equal to -1, so that it can drive the acceleration of the expansion of the universe. Another explanation is that dark energy is a form of dynamical energy field, called the *quintessence* field (Linder 2008). Therefore the potential energy of the field can be a trigger for the acceleration of the scale factor. The difference from the cosmological constant is that the quintessence field can vary in space and time. A scalar field can be one example based on the standard model of elementary particles (Koivisto and Mota 2007). There are substantial amount of possiblities for dark energy and also alternatives to dark energy which are aimed to explain the observational data as well (Ishak et al. 2008; Mattsson 2010).

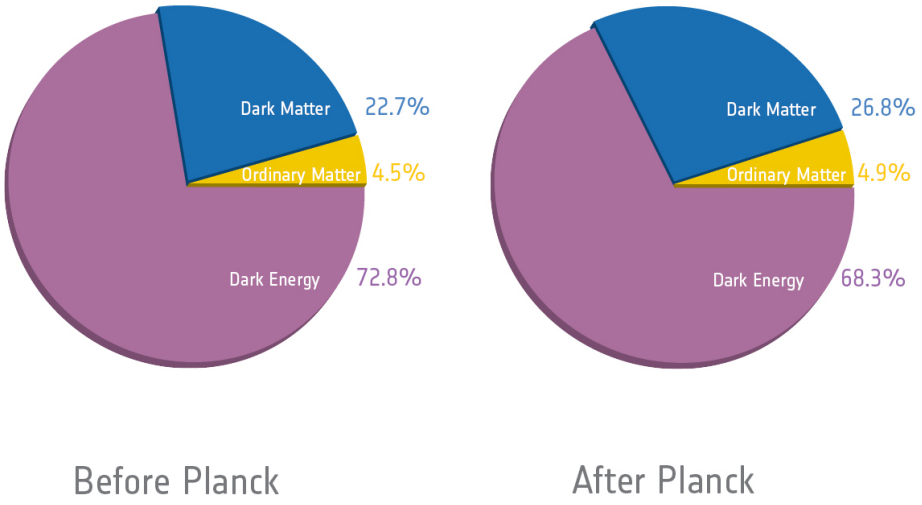

Figure 1.1 New cosmic inventory data from Planck's high-precision CMB map (Planck Collaboration et al. 2013). The 'before Planck' figure is based on the WMAP nine-year data release presented by (Hinshaw et al. 2012).

Chapter 2

Phase plane analysis

The phase plane provides a visualization of the qualitative behavior of the differential equation system (Graham and McRuer 1961). It is a great tool to understand especially nonlinear systems because it is not often that nonlinear systems have analytical solutions. The phase plane also gives us a physical insight of the system. In order to understand the phase plane, we start with a two-dimensional system of differential equations as a simple but very useful example

$$\begin{aligned} x' &= p(x, y) \\ y' &= q(x, y) \end{aligned} \tag{2.1}$$

where x and y are states of the system and p and q are nonlinear functions of the states [1]. Basically the phase plane is the plane having x and y as its coordinates not a time t. It can be written as

$$\frac{dy}{dx} = \frac{q(x, y)}{p(x, y)} \tag{2.2}$$

The equilibrium solution (or singular point) of the system, for example, is

$$\begin{aligned} p(x_0, y_0) &= 0 \\ q(x_0, y_0) &= 0 \end{aligned} \tag{2.3}$$

Now we look at the behavior of a equilibrium point under small perturbations

$$\begin{aligned} x &= x_0 + \delta x \\ y &= y_0 + \delta y \end{aligned} \tag{2.4}$$

[1] Previously we defined two different time variables, cosmic time which is denoted as dot and e-folding time which is denoted as prime. However here we don't distinguish these two. The prime denotes differentiation with respect to the general time term t here.

We assume that the perturbations are so small that it is sufficient to expand the equations to first order in them. Differentiating (2.4) with respect to t gives

$$\begin{aligned} x' &= \delta x' \\ y' &= \delta y' \end{aligned} \tag{2.5}$$

where the derivatives of the perturbations to the linear order are

$$\begin{aligned} \delta x' &= \left.\frac{\partial p}{\partial x}\right|_{x_0} \delta x + \left.\frac{\partial p}{\partial y}\right|_{y_0} \delta y \\ \delta y' &= \left.\frac{\partial q}{\partial x}\right|_{x_0} \delta x + \left.\frac{\partial q}{\partial y}\right|_{y_0} \delta y \end{aligned} \tag{2.6}$$

By setting in a new notation as below

$$a \equiv \left.\frac{\partial p}{\partial x}\right|_{x_0}, \quad b \equiv \left.\frac{\partial p}{\partial y}\right|_{y_0}, \quad c \equiv \left.\frac{\partial q}{\partial x}\right|_{x_0}, \quad d \equiv \left.\frac{\partial q}{\partial y}\right|_{y_0} \tag{2.7}$$

then (2.6) becomes

$$\begin{aligned} \delta x' &= a\,\delta x + b\,\delta y \\ \delta y' &= c\,\delta x + d\,\delta y \end{aligned} \tag{2.8}$$

which can be expressed to a matrix equation

$$\begin{pmatrix} \delta x' \\ \delta y' \end{pmatrix} = \begin{pmatrix} a & b \\ c & d \end{pmatrix} \begin{pmatrix} \delta x \\ \delta y \end{pmatrix} \tag{2.9}$$

In linear algebra, every square matrix is associated with a characteristic polynomial (Blyth and Robertson 2002). This is very useful since the important properties of matrix such as eigenvalues, determinant and trace are in the characteristic polynomial. Let us define (2.9) as follows

$$\frac{d\mathbf{x}}{dt} = \mathbf{M}\mathbf{x} \quad \text{where} \quad \mathbf{x} \equiv \begin{pmatrix} \delta x \\ \delta y \end{pmatrix}, \mathbf{M} \equiv \begin{pmatrix} a & b \\ c & d \end{pmatrix} \tag{2.10}$$

Then the characteristic equation of a matrix $\mathbf{M}$ is

$$\det\left[\,\mathbf{M} - \lambda\mathbf{I}\,\right] = 0 \tag{2.11}$$

where det is the determinant and $\mathbf{I}$ is the identity matrix. The eigenvalues of the matrix $\mathbf{M}$ is exactly the solution of the characteristic equation which is λ. Substituting the matrix (2.10) to (2.11) gives

$$\det\begin{bmatrix} a-\lambda & b \\ c & d-\lambda \end{bmatrix} = 0 \tag{2.12}$$

Then we find our characteristic equation of the matrix $\mathbf{M}$

$$\lambda^2 - (a+d)\lambda + (ad - bc) = 0 \tag{2.13}$$

where $a+d$ is the trace and $ad-bc$ is the determinant of the coefficient matrix $\mathbf{M}$. We can rewrite this relationship more explicitly as follows

$$\lambda = \frac{1}{2}\left(a+d \pm \sqrt{(a+d)^2 - 4(ad-bc)}\right) \tag{2.14}$$

The eigenvectors are defined as $\mathbf{Mx} = \lambda\mathbf{x}$. The eigenvalues are the powers of the exponential components and the eigenvectors are coefficients. Then the general solution of the system will be

$$\mathbf{x}(t) = c_1\mathbf{k}_1 e^{\lambda_1 t} + c_2\mathbf{k}_2 e^{\lambda_2 t} \tag{2.15}$$

where $\mathbf{k}_1$ and $\mathbf{k}_2$ are linearly independent eigenvectors. c_1 and c_2 are undetermined constants which can be solved if we have an initial condition of the system. The behavior of the solutions depends on the characteristic of the eigenvalues λ_1 and λ_2. These eigenvalues completely reveal the stability properties of the equilibrium point of the system. We consider the following possible cases where two eigenvalues are real and distinct.

- If the signs of eigenvalues are both negative, the trajectories from the entire phase plane converges to the equilibrium point [2] which is a *stable node* or an *attractor*. The phase portrait of an asymptotically stable point is shown in Fig. 2.1. Here the example matrix $((-1,0),(0,-2))$ is used, which has the negative eigenvalues -1 and -2.

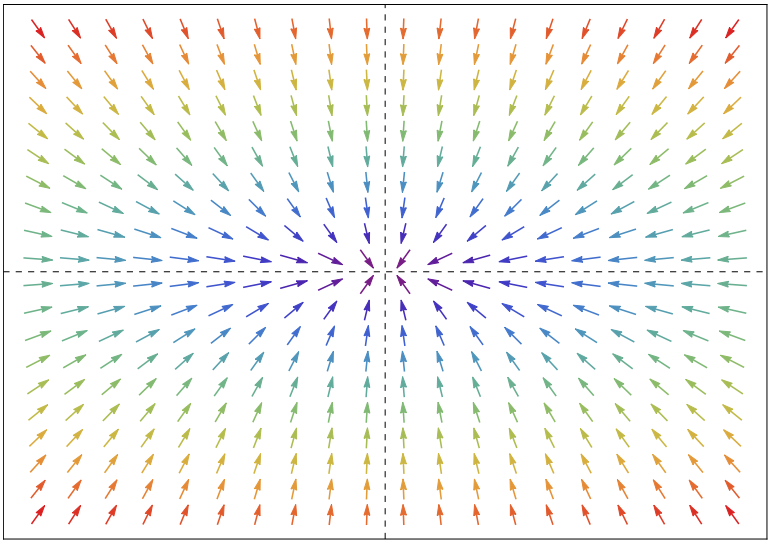

Figure 2.1 Phase portrait for asymptotically stable node. The origin is the equilibrium point and the axes are δx and δy, respectively.

[2] The equilibrium point does not have to be at the origin. Even if the equilibrium point is not at the origin, there is no loss of generality by this assumption. The shifted system can always be chosen without any behavioral change of the system.

- If the signs are all positive, the solution grows exponentially so they move away from the node as time increases. This equilibrium point is called an *unstable node* or a *repellor*. The phase portrait of an unstable point is shown in Fig. 2.2. Here the example matrix $((1,0),(0,2))$ is used, which has the positive eigenvalues 1 and 2.

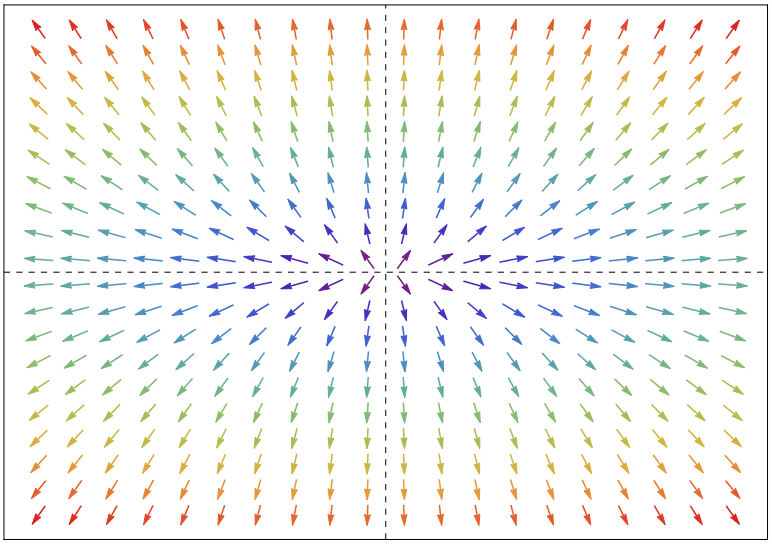

Figure 2.2 Phase portrait for unstable node. The origin is the equilibrium point and the axes are δx and δy, respectively.

Furthermore, there can be a special case that two real eigenvalues are equal, then the general solution (2.15) becomes

$$\mathbf{x}(t) = (c_1\mathbf{k}_1 + c_2\mathbf{k}_2)e^{\lambda t} \tag{2.16}$$

In this case, all trajectories are the straight lines towards origin. The origin is called a proper node. In addition to the equal eigenvalues if the matrix $\mathbf{M}$ has only one independent eigenvector $\mathbf{k}$, then the general solution (2.15) becomes

$$\mathbf{x}(t) = c_1\mathbf{k}e^{\lambda t} + c_2(\mathbf{k}t + \mathbf{k}_\mathrm{g})e^{\lambda t} \tag{2.17}$$

where $\mathbf{k}_\mathrm{g}$ is a generalized eigenvector defined as

$$(\mathbf{M} - \lambda\mathbf{I})\mathbf{k}_\mathrm{g} = \mathbf{k} \tag{2.18}$$

In this case the origin is called an *improper node*. If the matrix $\mathbf{M}$ have two linearly independent eigenvectors, the origin is a *proper node*.

- If the eigenvalues have opposite sign, one solution will approach the equilibrium point from one direction but diverge away from the another direction. So there exist both stable and unstable trajectories. The equilibrium point

in this case is termed a *saddle point*. It is considered as an unstable point. The phase portrait of a saddle point is shown in Fig. 2.3. Here the example matrix $((1,2),(3,2))$ is used, which has the opposite sign of eigenvalues -1 and 4.

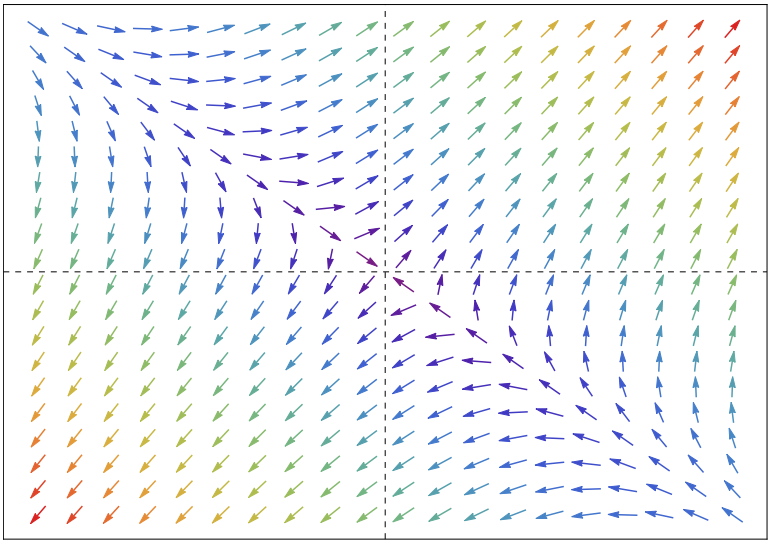

Figure 2.3 Phase portrait for unstable saddle point. The origin is the equilibrium point and the axes are δx and δy, respectively.

Now let us look at the cases that the eigenvalues are not real anymore.

- If the eigenvalues are complex conjugates, for example $\lambda = \alpha \pm \beta i$ with eigenvectors $\mathbf{k} = \mathbf{A} \pm \mathbf{B}i$, we obtain two linearly independent solutions

$$\begin{aligned} \mathbf{x}_1(t) &= (\mathbf{A}\cos\beta t - \mathbf{B}\sin\beta t)\, e^{\alpha t} \\ \mathbf{x}_2(t) &= (\mathbf{B}\cos\beta t + \mathbf{A}\sin\beta t)\, e^{\alpha t} \end{aligned} \tag{2.19}$$

Then the general solution becomes

$$\mathbf{x}(t) = c_1\mathbf{x}_1(t) + c_2\mathbf{x}_2(t) \tag{2.20}$$

Note that it has a nonzero real part. The equilibrium point becomes a *spiral point* and the stability depends on the sign of the real part α. It diverges for negative real part and converges for positive real part. The phase portrait of an asymptotically stable spiral point is shown in Fig. 2.4. The example matrix $((0,1),(-1,-1))$ is used and it has the eigenvalues $-(1 \pm \sqrt{3}i)/2$ and the negative real number $-1/2$. Also the phase portrait of an unstable spiral point is shown in Fig. 2.5. The example matrix $((0,1),(-1,1))$ is used, which has the eigenvalues $(1 \pm \sqrt{3}i)/2$ and the positive real number $1/2$.

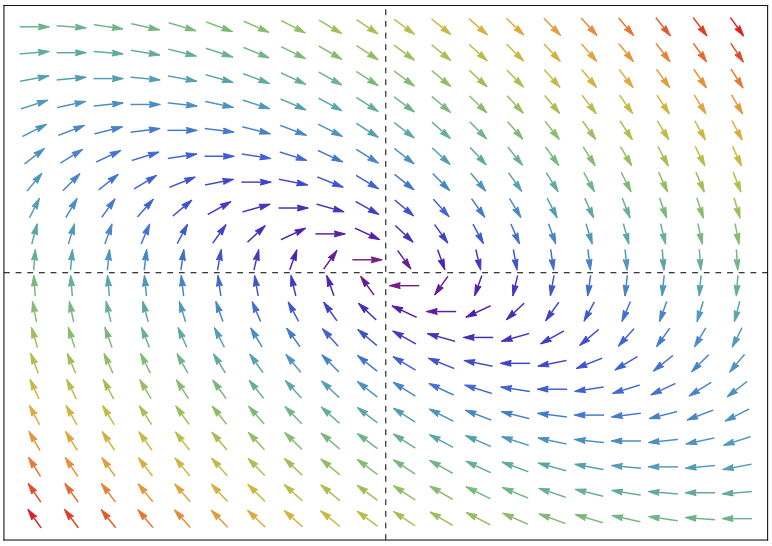

Figure 2.4 Phase portrait for asymptotically stable spiral point when the real part $\alpha < 0$. The origin is the equilibrium point and the axes are δx and δy, respectively.

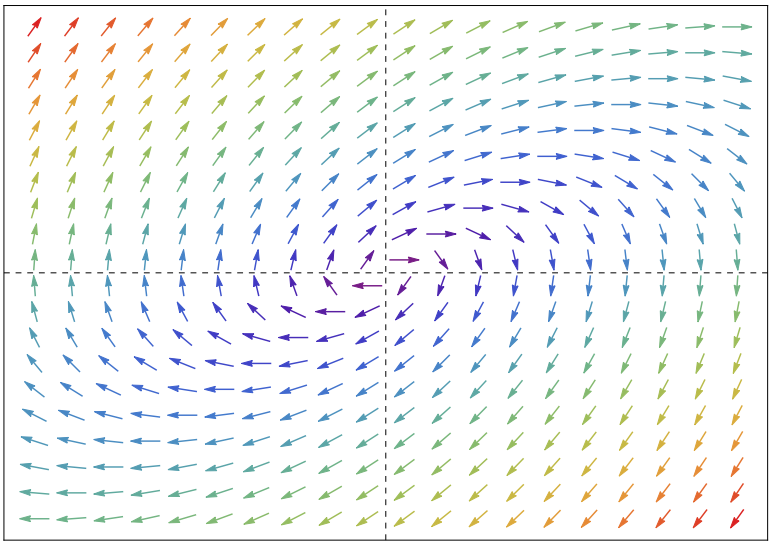

Figure 2.5 Phase portrait for unstable spiral point when the real part $\alpha > 0$. The origin is the equilibrium point and the axes are δx and δy, respectively.

- If the both eigenvalues are pure imaginary values for an example of $\lambda = \pm\beta i$ with eigenvectors $\mathbf{k} = \mathbf{A} \pm \mathbf{B}i$, we find two linearly independent solutions

$$\begin{aligned} \mathbf{x}_1(t) = &\quad (\mathbf{A}\cos\beta t - \mathbf{B}\sin\beta t) \\ \mathbf{x}_2(t) = &\quad (\mathbf{B}\cos\beta t + \mathbf{A}\sin\beta t) \end{aligned} \tag{2.21}$$

Then the general solution becomes

$$\mathbf{x}(t) = c_1\mathbf{x}_1(t) + c_2\mathbf{x}_2(t) \tag{2.22}$$

Since the real part of the eigenvalue is zero, this is a periodic solution. The equilibrium point is a stable center. The phase portrait of a stable center is shown in Fig. 2.6. The example matrix used is $((0,1),(-1,0))$ which has the complex eigenvalue i.

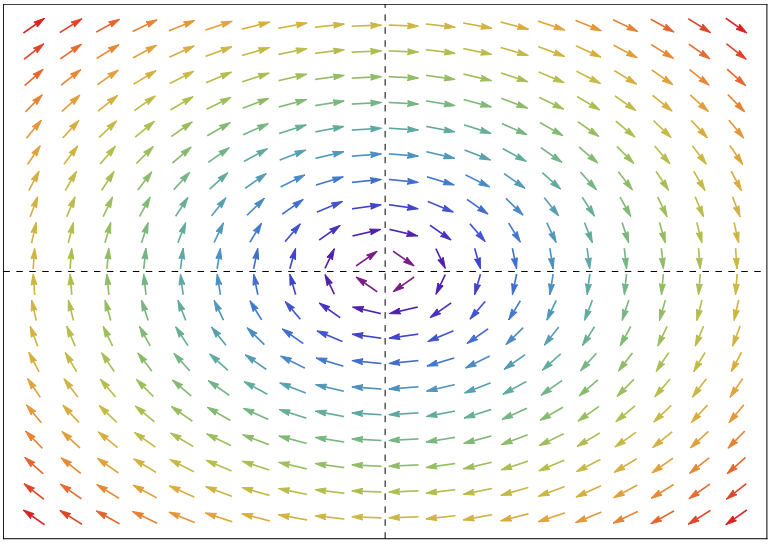

Figure 2.6 Phase portrait for stable center when the real part is zero. The origin is the equilibrium point and the axes are δx and δy, respectively.

The stable node in Fig. 2.1 and the stable spiral point in Fig. 2.4 are asymptotically stable. In other words, no matter where the trajectories begin, they all end up at the equilibrium at last. On the other hand, the stable center in Fig. 2.6 does not show any asymptotic characteristics. All the trajectories remain in their own orbit, therefore they never reach the equilibrium point.

The possibilities of the stability conditions are summarized in Table 2.1.

Eigenvalues	Equilibrium point
Real and negative	Stable node
Real and positive	Unstable node
Real and opposite signs	Saddle point
Complex and negative real part	Stable spiral point
Complex and positive real part	Unstable spiral point
Complex and zero real part	Stable center

Table 2.1 Possible cases of the stability conditions according to the eigenvalues.

Chapter 3

Anisotropic Equation of State

In this chapter, we start by taking a look at anisotropic cosmology models and setting up metrics. Then we rewrite the Einstein equations in terms of our dynamic variables which yields the generalized Friedmann equation. Consequently the evolution equations for each variables are derived. Phase plane analysis is shortly reviewed in given system as well.

3.1 Anisotropic cosmology

The possible cosmological symmetries for isotropy can be classified into isotropic, locally rotationally symmetric (LRS) and anisotropic at a general point. If it is isotropic, there are no curvature quantities and all observations at every point are isotropic. This is the Friedmann–Lemaître–Robertson–Walker (FLRW) geometry. If it is LRS which is proposed in (Mimoso and Crawford 1993), kinematical quantities are rotationally symmetric to a preferred spatial direction. All observations at every point are rotationally symmetric to this preferred direction. More specifically, in three-dimensions there are two different kinds rotational symmetry. If there is no change when rotating about one axis then it is a cylindrical symmetry and if there is no change for any rotation, it is a spherical symmetry. Axisymmetry in this sense refers to a cylindrical symmetry. If it is anisotropic, there are no rotational symmetries and observations in each direction are different from observations in each other direction (Ellis and van Elst 1999). Our framework is set up in spatially homogeneous LRS metrics. To make it simple, the axisymmetric LRS class is chosen here (Koivisto et al. 2011):

$$ds^2 = -dt^2 + b^2(t)dy^2 + a^2(t)\left[d\xi^2 + \frac{1}{|k|}S^2(|k|^{\frac{1}{2}}\xi)d\phi^2\right] \tag{3.1}$$

where

$$S(x) \equiv \begin{cases} \sin x & \text{for } k > 0 \\ x & \text{for } k = 0 \\ \sinh x & \text{for } k < 0 \end{cases} \tag{3.2}$$

and the Ricci scalar of spatial hypersurfaces ${}^3R$ is related to the curvature k :

$${}^3R = \frac{2k}{a^2} \tag{3.3}$$

The case $S(x) = \sin x$ corresponds to the Kantowski-Sachs metric with spatial sections of the form of the product $\mathcal{R} \times \mathcal{S}^2$. In all cases, the line $\mathcal{R}$ is parametrized by the coordinate y. In particular, here ξ and ϕ should be considered as angular coordinates on the two sphere $\mathcal{S}^2$. The second case $S(x) = x$ corresponds to the Bianchi I geometry, for which spatial sections take the form $\mathcal{R} \times \mathcal{R}^2$. With the line $\mathcal{R}$ in this case the functions ξ and ϕ should be thought of as cylindrical coordinates on the plane $\mathcal{R}^2$. For $S(x) = \sinh x$ we have Bianchi III metric with spatial sections of the form $\mathcal{R} \times \mathcal{H}^2$. In this case, the functions ξ and ϕ should be considered as hyperbolic coordinates on the two hyperboloid $\mathcal{H}^2$. The Bianchi I metric contains flat FRW geometry as a special case when $a(t) = b(t)$, but the other two cases are anisotropic forever, since their sectional curvatures are never equal at the same time.

3.2 Phase space variables

We are ready to set up our phase space variables. The expansion rate of universe is characterized by

$$H_a = \frac{\dot{a}}{a} \quad \text{and} \quad H_b = \frac{\dot{b}}{b} \tag{3.4}$$

where overdot denotes the derivative with respect to coordinate time t. In the limit of $H_a = H_b$ the isotropic flat Friedmann universe is recovered. The mean expansion rate can be determined as an average Hubble rate H

$$H \equiv \frac{2H_a + H_b}{3} \tag{3.5}$$

The differences of expansion rates can be expressed as a shear anisotropy parameter S (Barrow 1997)

$$S \equiv \frac{H_a - H_b}{H} \tag{3.6}$$

which is Hubble-normalized and dimensionless. A notation here is in the coordinate formalism and the equations are in terms of the metric components for simpler and more transparent analysis. Alternative parametrization in covariant expressions was conducted in Koivisto and Mota (2008). We consider a universe as a

two-fluid system filled with a perfect fluid (dark matter) and an imperfect fluid (dark energy). Now we can generalize the results that are obtained on a FRW universe from first chapter. The case we are interested in is that there is no interactions between a perfect fluid and a fluid with and anisotropic pressure. The perfect fluid energy-momentum tensor characterized by its rest frame mass density ρ and isotropic pressure $\omega\rho$ is simply

$$T^{\mu}{}_{\nu} = \text{diag}(-1,\ \omega,\ \omega,\ \omega)\rho \tag{3.7}$$

where ω is the equation of state parameter of matter, $\omega = 0$ for dust and $\omega = 1/3$ for radiation. In the chosen framework the off-diagonal elements of Einstein tensor vanish, so the energy-momentum tensor should be diagonalized. If the pressure in each coordinate direction is different, the anisotropy of the pressure can be parametrized by the dimensionless skewness parameter γ

$$3\gamma \equiv \frac{p_x - p_y}{\rho} = \frac{p_z - p_y}{\rho} \tag{3.8}$$

Then the energy-momentum tensor of dark energy is

$$T^{\mu}_{(\mathrm{B})\nu} = \text{diag}(-1,\ \omega_{\mathrm{B}} + 3\gamma,\ \omega_{\mathrm{B}},\ \omega_{\mathrm{B}} + 3\gamma)\rho_{\mathrm{B}} \tag{3.9}$$

where ω_{B} is the equation of state parameters of background. With the given matter contents, the Einstein field equations

$$G^{\mu}{}_{\nu} = 8\pi G(T^{\mu}{}_{\nu} + T^{\mu}_{(\mathrm{B})\nu}) \tag{3.10}$$

can be written as (henceforth $8\pi G \equiv 1$)

$$\frac{\ddot{a}}{a} + \frac{\ddot{b}}{b} + \frac{\dot{a}}{a}\frac{\dot{b}}{b} = -P - P_{\mathrm{B}} \tag{3.11}$$

$$2\frac{\ddot{a}}{a} + \frac{k + \dot{a}^2}{a^2} = -P - P_{\mathrm{B}} - L_{\mathrm{B}} \tag{3.12}$$

$$2\frac{\dot{a}}{a}\frac{\dot{b}}{b} + \frac{k + \dot{a}^2}{a^2} = \rho + \rho_{\mathrm{B}} \tag{3.13}$$

where $P = \omega\rho$, $P_{\mathrm{B}} = \omega_{\mathrm{B}}\rho_{\mathrm{B}}$, and $L_{\mathrm{B}} = 3\gamma\rho_{\mathrm{B}}$, respectively. The continuity equations of a fluid are defined by the divergence equation which is a statement of conservation of energy and conservation of linear momentum.

$$\dot{\rho} = -3H(1 + \omega)\rho \tag{3.14}$$

$$\dot{\rho_{\mathrm{B}}} = -H[\,3(1 + \omega_{\mathrm{B}}) + \gamma(3 - 2S)]\rho_{\mathrm{B}} \tag{3.15}$$

It shows that the densities fall in proportion to the comoving volume as

$$\rho \propto (a^2 b)^{-1-\omega} \quad \text{and} \quad \rho_{\mathrm{B}} \propto (a^2 b)^{-1-\omega_{\mathrm{B}}} a^{6\gamma} \tag{3.16}$$

3.3 Evolution equations

We define a curvature parameter K as our new phase space variable which scales as a^{-2}

$$K \equiv \frac{k}{a^2 H^2} \tag{3.17}$$

In the case of $K = 0$ the flat FRW universe is recovered. A curved universe will be studied separately. The dimensionless density parameters may be defined as follows

$$\Omega \equiv \frac{\rho}{3H^2} \quad \text{and} \quad \Omega_{\text{B}} \equiv \frac{\rho_{\text{B}}}{3H^2} \tag{3.18}$$

By introducing these density parameters we can quantify the amount of matter in accordance with the standard cosmology as a fraction of matter contribution inversely proportional to the square of the average Hubble rate H. As the time variable we will use an average e-folding time scale N rather than t

$$N \equiv \frac{1}{3}\log(a^2 b) \tag{3.19}$$

in relation to the cosmic time scale t

$$\frac{d}{dN} = \frac{1}{H}\frac{d}{dt} \tag{3.20}$$

In the following the derivative of a function with respect to N will be denoted by prime. In the case of $H_a = H_b$, the e-folding time becomes $N = \log a$ which describes isotropic expansion. It is also useful to employ the so-called slow-roll parameter ϵ by

$$\epsilon \equiv \frac{3}{2}(1 + \omega_{\text{eff}}) = -\frac{\dot{H}}{H^2} \tag{3.21}$$

where the effective equation of state $\omega_{\text{eff}} = \Sigma\ \omega_i \Omega_i$. Using the relation of the definitions of the average Hubble rate (3.5) and the shear (3.6)

$$H_a = \frac{H}{3}(S + 3) \quad \text{and} \quad H_b = \frac{H}{3}(3 - 2S) \tag{3.22}$$

and rewriting the Einstein equation (3.13) in terms of our dynamic variables, the shear anisotropy S, the two density parameters Ω and Ω_{B}, and the curvature K, yields the generalized Friedmann equation

$$S^2 = 3K - 9(\Omega + \Omega_{\text{B}} - 1) \tag{3.23}$$

Rewriting (3.13) gives

$$\frac{\ddot{a}}{a} = \dot{H}_a + H_a^2 \quad \text{and} \quad \frac{\ddot{b}}{b} = \dot{H}_b + H_b^2 \tag{3.24}$$

Substituting the slow-roll parameter (3.21) and (3.24) in the first field equation (3.11) and combining it with the second field equation (3.12) gives

$$\epsilon = \frac{3}{2}\left[1 + \omega\Omega + (\omega_{\mathrm{B}} + \gamma)\Omega_{\mathrm{B}} + \frac{1}{9}(S^2 + K)\right] \tag{3.25}$$

The above can be confirmed by the comparison with (3.21). Then from the equations (3.11) and (3.12) with (3.25) by getting rid of S^2 we can finally obtain the evolution equation for S

$$S' = (\epsilon - 3)S - 9\gamma\Omega_{\mathrm{B}} - K \tag{3.26}$$

By the definitions (3.18) and (3.21) and the continuity equations (3.14) and (3.15) the evolution equations for Ω and Ω_{B} turn out to be

$$\Omega' = [2\epsilon - 3(1 + \omega)]\,\Omega \tag{3.27}$$
$$\Omega'_{\mathrm{B}} = [2\epsilon - 3(1 + \omega_{\mathrm{B}}) + \gamma(2S - 3)]\,\Omega_{\mathrm{B}} \tag{3.28}$$

Similarly, starting from the definition of the curvature parameter (3.17) and employing (3.21) and (3.22), we find our curvature evolution equation at last.

$$K' = \frac{2}{3}(3\epsilon - S - 3)K \tag{3.29}$$

One can see from the evolution equations that the anisotropic matter generates the shear and the curvature. If $\Omega = 0$, then $\Omega' = 0$ as it is shown from (3.28), therefore it does not evolve from zero. In other words, Ω stays zero if it ever hits zero. The same for Ω_{B} and K as well. However shear S is sourced by the other properties. The results can be double-checked by plugging all the evolution equations into the derivative of the Friedmann equation (3.23)

$$2SS' - 3K' + 9(\Omega' + \Omega'_{\mathrm{B}}) = 0 \tag{3.30}$$

3.4 The background as a dynamical system

It has been shown that a model beginning from a matter-dominated scaling solution to an accelerating scaling solution in the Friedmann-Lemaître universe has difficulty proving the coincidence problem. Opening the possibility to have different expansion rates might help us understand why and how the cosmic acceleration began. Hence we study the asymptotic behaviors of the universe.

We start with some assumptions to make it as simple as possible. Our universe is initially isotropic enough, however it expands anisotropically due to the skewness of dark energy. Let us look at the system of Bianchi I, the simplest one among all

Bianchi models, by setting $K = 0$. Our system is axisymmetric with respect to y axis and no coupling between the components Ω and Ω_B. To find the fixed point of the system we assume that the evolution equations are constants that guarantee

$$S' = \Omega' = \Omega'_{\mathrm{B}} = 0 \tag{3.31}$$

We assume constant equation of state and skewness parameter as well

$$\omega' = \omega'_{\mathrm{B}} = \gamma' = 0 \tag{3.32}$$

Therefore the phase variables are only proportional to the perturbations. The fixed points are found by solving the evolution equations which are simply ordinary differential equations. We can simplify the equations further by eliminating Ω in ϵ from the generalized Einstein equation (3.23).

$$\Omega = 1 - \Omega_{\mathrm{B}} - \frac{1}{9}S^2 \tag{3.33}$$

The slow-roll parameter ϵ can be removed in the process. Considering our universe is flat, there are only two phase variables left, S and Ω_{B}. It turns out that our system has five fixed points. The stability of these fixed points will tested by adding disturbances. Now we add small perturbations and write full quantities as

$$\begin{aligned} S &= S_0 + \delta S \\ \Omega_{\mathrm{B}} &= \Omega_{\mathrm{B0}} + \delta\Omega_{\mathrm{B}} \end{aligned} \tag{3.34}$$

where S_0 and Ω_{B0} are the background values which are our fixed points. By differentiating (3.34) with respect to the e-folding time, we can make use of (3.31). The background values would be then zero combining (3.31) and (3.34) gives another useful relation

$$\begin{aligned} S' &= \delta S' = 0 \\ \Omega'_{\mathrm{B}} &= \delta\Omega'_{\mathrm{B}} = 0 \end{aligned} \tag{3.35}$$

According to the assumption, the perturbations are very small, so it is sufficient to expand the equations to first order. With mentioned assumptions and (3.25), (3.26) and (3.28) we can derive $\delta S'$ and $\delta\Omega'_{\mathrm{B}}$ in the perturbed terms of δS and $\delta\Omega_{\mathrm{B}}$ exactly like (2.8)

$$\begin{aligned} \delta S' &= B_1\,\delta S + B_2\,\delta\Omega_{\mathrm{B}} \\ \delta\Omega'_{\mathrm{B}} &= B_3\,\delta S + B_4\,\delta\Omega_{\mathrm{B}} \end{aligned} \tag{3.36}$$

which can be written in a matrix form like (2.9)

$$\begin{pmatrix} \delta S' \\ \delta\Omega'_{\mathrm{B}} \end{pmatrix} = \begin{pmatrix} B_1 & B_2 \\ B_3 & B_4 \end{pmatrix} \begin{pmatrix} \delta S \\ \delta\Omega_{\mathrm{B}} \end{pmatrix} \tag{3.37}$$

The condition (3.35) defines the left-hand side of (3.37) zero. Then from the characteristic equations we can find the eigenvalues which will give the information about what kind of fixed point it is.

Chapter 4

Fixed points in a flat geometry

4.1 Analytical stability analysis

Our framework for a flat universe is set up in the Bianchi I metric. This model describes the simplest homogeneous and anisotropic universe (Ellis 2006). Usually the Bianchi models are isotropized, unless anisotropic matter sources may be needed (Ellis and van Elst 1999). If a universe is filled with perfect fluid, this becomes a FRW universe after all (Jacobs 1968). Since the modern cosmological observations imply that the universe is isotropic to about 10^{-5} (Copi et al. 2010) and it is not likely to have growing anisotropies, the models that isotropize have been more studied. Therefore it seems to need a fine-tuned cosmology that agrees with non-isotropization and the observational data. However there has been evidences against the presumptions mentioned above. So we analyze for fixed points here in the more general point of direction-dependent expansion rates. In the axisymmetric case the line element of a BI universe can be written as

$$ds^2 = -dt^2 + a^2(t)dx^2 + b^2(t)dy^2 + a^2(t)dz^2 \tag{4.1}$$

where there are two scale factors and therefore two volume expansion rates, respectively. With previous assumptions our system turns out to have 5 fixed points.

4.1.1 The FLRW solution

$$\Omega = 1, \quad \Omega_{\mathrm{B}} = 0, \quad S = 0 \tag{4.2}$$

It describes a matter-dominated, flat and isotropic universe. Following the calculation introduced in Sec. 3.4 we find two eigenvalues

$$\left\{ \frac{3}{2}(\omega - 1), \;\; 3(\omega - \omega_{\mathrm{B}} - \gamma) \right\}$$

For simplicity's sake, we assume $\omega < 1$. When $\omega < \omega_B + \gamma$ the FLRW solution is a stable node, otherwise a saddle point.

There are the phase portraits in this fixed point. The following phase portraits are generated from the matrix as in 3.37:

$$\begin{bmatrix} \frac{3}{2}(\omega - 1) & 9\gamma \\ 0 & 3(\omega - \omega_B - \gamma) \end{bmatrix}$$

The center is the origin and the axes are δS and $\delta\Omega_B$, respectively. It gives the visualization of qualitative behavior. The figure at left side clearly shows a general behavior in totally however does not show any direction, so the additional figure at right side is added for better understanding. The phase portrait in the case of $\gamma = 0.25\,, \omega = 0$ and $\omega_B = -1$ is shown in Fig. 4.1. As it is shown that trajectories approch to the origin horizontally but spread out from it, which proves it is a saddle point in this case. It agrees with the stability condition we derived above. Since $\omega > \omega_B + \gamma$, this is expected to be a saddle point. The following phase portrait in Fig. 4.2 is the case of $\gamma = -0.25\,, \omega = 0$ and $\omega_B = -1$. According to the stability condition $\omega > \omega_B + \gamma$, this is expected to be a saddle point. The phase portrait in the case of $\gamma = 2\,, \omega = 0$ and $\omega_B = -1$ is shown in Fig. 4.3. Trajectories starting from everywhere converge to the origin. It shows the behavior of a stable point which corresponds to the stability condition $\omega < \omega_B + \gamma$. The following phase portrait in Fig. 4.4 is the case of $\gamma = -2\,, \omega = 0$ and $\omega_B = -1$. It shows the behavior of a saddle point. From the stability condition $\omega > \omega_B + \gamma$, it is expected to be a saddle point.

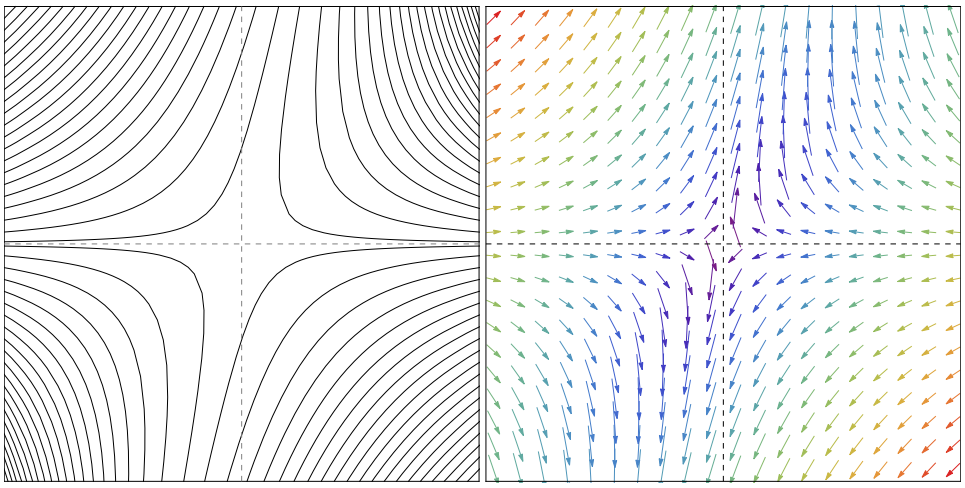

Figure 4.1 Phase portrait in the case of $\gamma = 0.25\,, \omega = 0$ and $\omega_B = -1$. The center is the origin and the axes are δS and $\delta\Omega_B$, respectively. It shows the behavior of a saddle point.

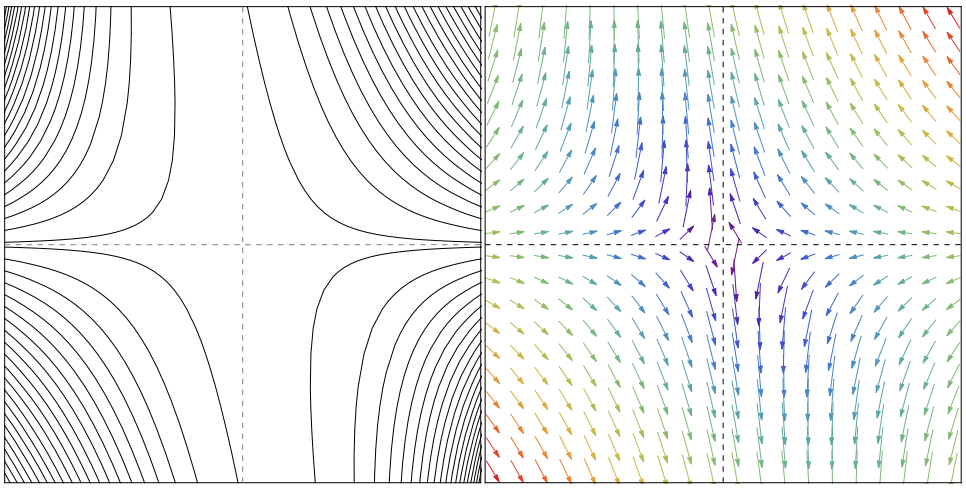

Figure 4.2 Phase portrait in the case of $\gamma = -0.25$, $\omega = 0$ and $\omega_{\mathrm{B}} = -1$. The center is the origin and the axes are δS and $\delta\Omega_{\mathrm{B}}$, respectively. It shows the behavior of a saddle point as well.

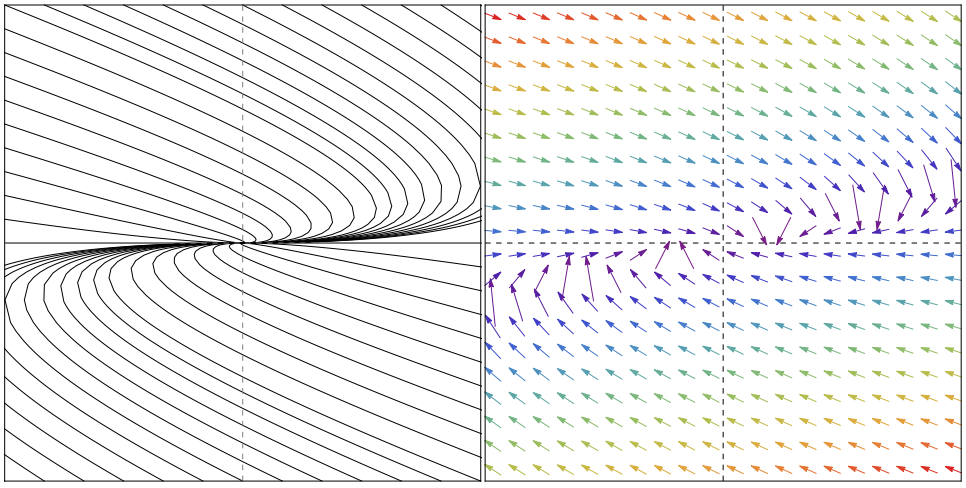

Figure 4.3 Phase portrait in the case of $\gamma = 2$, $\omega = 0$ and $\omega_{\mathrm{B}} = -1$. The center is the origin and the axes are δS and $\delta\Omega_{\mathrm{B}}$, respectively. It shows the behavior of a stable point.

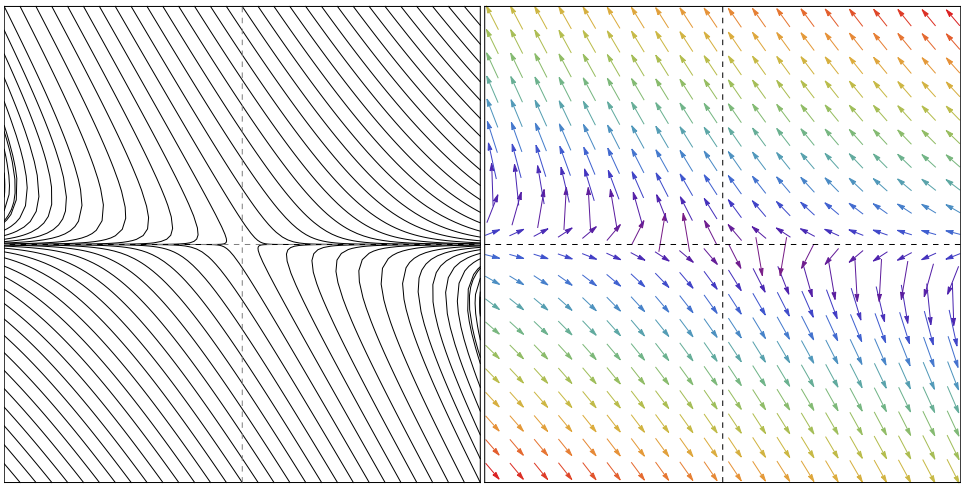

Figure 4.4 Phase portrait in the case of $\gamma = -2$, $\omega = 0$ and $\omega_{\mathrm{B}} = -1$. The center is the origin and the axes are δS and $\delta\Omega_{\mathrm{B}}$, respectively. It shows the behavior of a saddle point.

4.1.2 An anisotropically expanding empty universe

$$\Omega = 0, \quad \Omega_{\mathrm{B}} = 0, \quad S = \pm 3 \tag{4.3}$$

The universe in this case is shear-dominated. In the case of $S = 3$, the eigenvalues are

$$\{3(1-\omega),\ \ 3(1+\gamma-\omega_{\mathrm{B}})\}$$

and when $\gamma < \omega_{\mathrm{B}} - \omega$ it is a saddle point. In the case of $S = -3$, the eigenvalues are

$$\{3(1-\omega),\ \ 3(1-3\gamma-\omega_{\mathrm{B}})\}$$

and when $(\omega - \omega_{\mathrm{B}})/3 < \gamma$ it is a saddle point as well. Otherwise in both cases it is an unstable node. This is also called the Kasner solution which is an exact solution of the Einstein equations (Misner et al. 1973; Belinski and Verdaguer 2001). The Kasner metric can be described by

$$ds^2 = -dt^2 + t^{2p_1}dx^2 + t^{2p_2}dy^2 + t^{2p_3}dz^2 \tag{4.4}$$

where the Kasner exponents satisfy

$$p_1 + p_2 + p_3 = p_1^2 + p_2^2 + p_3^2 = 1 \tag{4.5}$$

As a consequence each hypersurface corresponding to constant t is a flat three-dimensional space. Since the volume element t is constantly increasing, it represents an expanding universe. It describes an anisotropic vacuum solution near the singularity, $t \to 0$ where the matter is negligible since $\rho/H^2 \approx 0$. Due to the axial symmetry, the two exponents p_1 and p_3 are equal in our system. We can find two

solutions in the present case. There can be two static directions and one expanding direction, corresponding $p_1 = p_3 = 0$ and $p_2 = 1$. Nextly, there can be two expanding directions and one contracting direction, corresponding $p_1 = p_3 = 2/3$ and $p_2 = -1/3$.

There are the phase portraits in this fixed point. First, the phase portraits of the case when $S = 3$ are shown. The following phase portraits are generated from the matrix as in 3.37:

$$\begin{bmatrix} 3(1-\omega) & \frac{9}{2}(\omega_{\mathrm{B}} - \omega + \gamma) \\ 0 & 3(1 - \omega_{\mathrm{B}} + \gamma) \end{bmatrix}$$

The center is the origin and the axes are δS and $\delta\Omega_{\mathrm{B}}$ again. The phase portrait in the case of $\gamma = 0.25\,, \omega = 0$ and $\omega_{\mathrm{B}} = -1$ is shown in Fig. 4.5. It shows that all the trajectories spread out from the origin which is the behavior of an unstable point. According to the stability condition $\gamma > \omega_{\mathrm{B}} - \omega$, it is expected to be an unstable point. The following phase portrait in Fig. 4.6 is the case of $\gamma = -0.25\,, \omega = 0$ and $\omega_{\mathrm{B}} = -1$. The stability condition agrees to the condition to be an unstable point, $\gamma > \omega_{\mathrm{B}} - \omega$. The phase portrait in the case of $\gamma = 2\,, \omega = 0$ and $\omega_{\mathrm{B}} = -1$ is shown in Fig. 4.7. It shows the behavior of an unstable point and it is also expected to be so by the stability condition $\gamma > \omega_{\mathrm{B}} - \omega$. The phase portrait in the case of $\gamma = -2.1\,, \omega = 0$ and $\omega_{\mathrm{B}} = -1$ is shown in Fig. 4.8. Note that $\gamma \neq -2$ here. The reason for using $\gamma = -2.1$ is to show a more recognizable figure because it is hard to see the change of directions from the original figure. First it is checked that a small change of the parameter does not make a drastic change of the result. Therefore from this figure we can understand the behavior of the orginal case as well. The original figure of the left panel only shows the straight lines. The right panel of the original figure also shows no change in $\delta\Omega_{\mathrm{B}}$ direction. This point is expected to be a saddle point from the stabiltiy condition $\gamma < \omega_{\mathrm{B}} - \omega$. From this figure we can see a very small but noticable change in $\delta\Omega_{\mathrm{B}}$ direction which makes it a saddle point. Next, when $S = -3$ the phase portraits are generated from the matrix :

$$\begin{bmatrix} 3(1-\omega) & -\frac{9}{2}(\omega_{\mathrm{B}} - \omega + 3\gamma) \\ 0 & 3(1 - \omega_{\mathrm{B}} - 3\gamma) \end{bmatrix}$$

The phase portrait in the case of $\gamma = 0.25\,, \omega = 0$ and $\omega_{\mathrm{B}} = -1$ is shown in Fig. 4.9. This shows a typical behavior of an unstable point. Trajectories diverge out from the orgin. It agrees with the result from the stability condition for an unstable point, $(\omega - \omega_{\mathrm{B}})/3 > \gamma$. The phase portrait in the case of $\gamma = -0.25\,,$ $\omega = 0$ and $\omega_{\mathrm{B}} = -1$ is shown in Fig. 4.10. This shows a typical behavior of an unstable point as well and also corresponds to the stability condition for an unstable point, $(\omega - \omega_{\mathrm{B}})/3 > \gamma$. The phase portrait in the case of $\gamma = 2\,, \omega = 0$ and $\omega_{\mathrm{B}} = -1$ is shown in Fig. 4.11. This shows a typical behavior of a saddle point diverging horizontally and converging vertically. This agrees with the result from the stability condition for a saddle point, $(\omega - \omega_{\mathrm{B}})/3 < \gamma$. The phase portrait in the case of $\gamma = -2\,, \omega = 0$ and $\omega_{\mathrm{B}} = -1$ is shown in Fig. 4.12. This is an unstable point as expected from the stability condition, $(\omega - \omega_{\mathrm{B}})/3 > \gamma$.

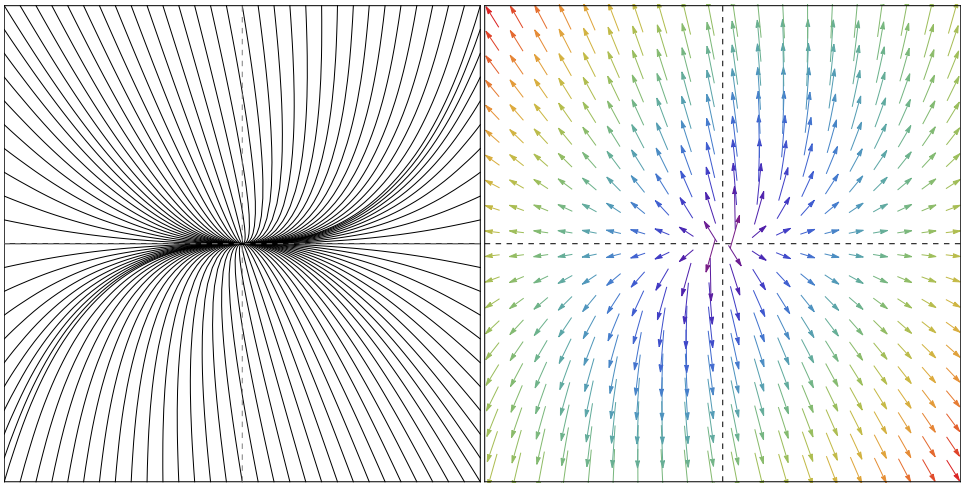

Figure 4.5 Phase portrait in the case of $\gamma = 0.25$, $\omega = 0$ and $\omega_{\rm B} = -1$ for the fixed point $S = 3$ and $\Omega_{\rm B} = 0$. The center is the origin and the axes are δS and $\delta\Omega_{\rm B}$, respectively. It is an unstable point.

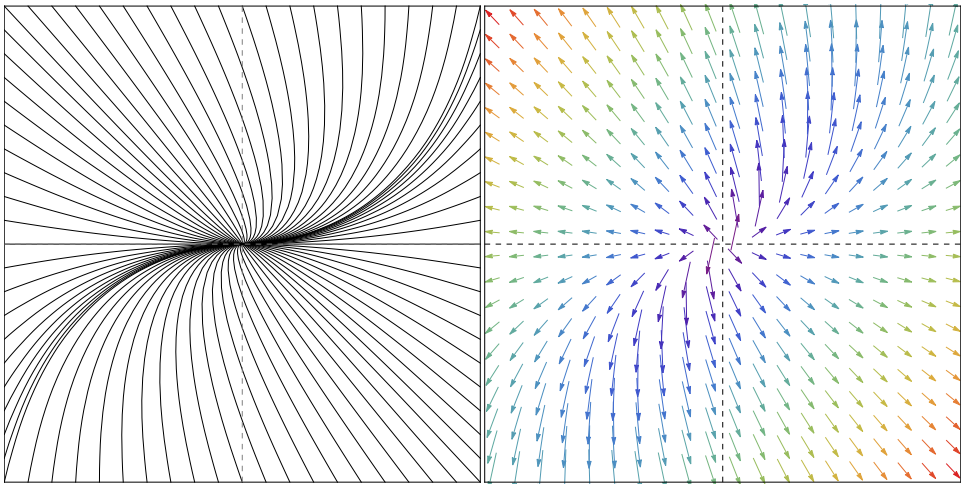

Figure 4.6 Phase portrait in the case of $\gamma = -0.25$, $\omega = 0$ and $\omega_{\rm B} = -1$ for the fixed point $S = 3$ and $\Omega_{\rm B} = 0$. The center is the origin and the axes are δS and $\delta\Omega_{\rm B}$, respectively. It is an unstable point as well.

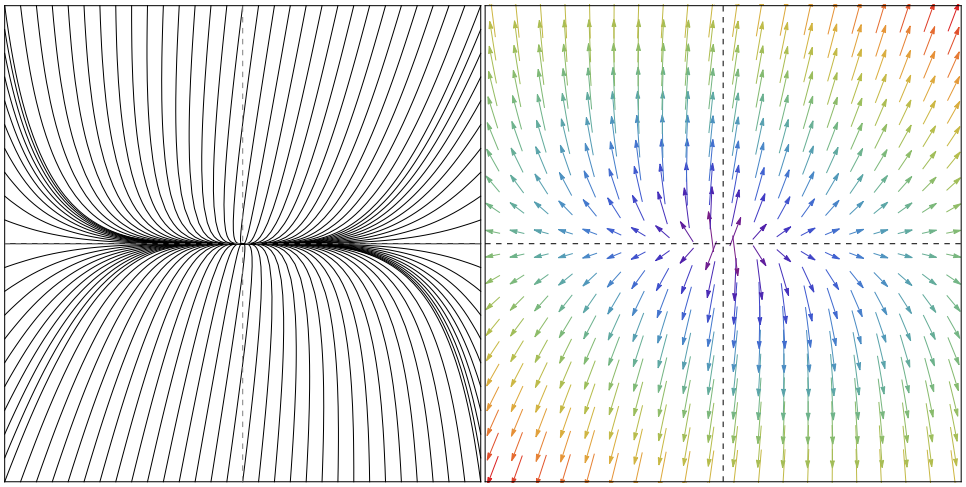

Figure 4.7 Phase portrait in the case of $\gamma = 2$, $\omega = 0$ and $\omega_{\mathrm{B}} = -1$ for the fixed point $S = 3$ and $\Omega_{\mathrm{B}} = 0$. The center is the origin and the axes are δS and $\delta\Omega_{\mathrm{B}}$, respectively. It is an unstable point as well.

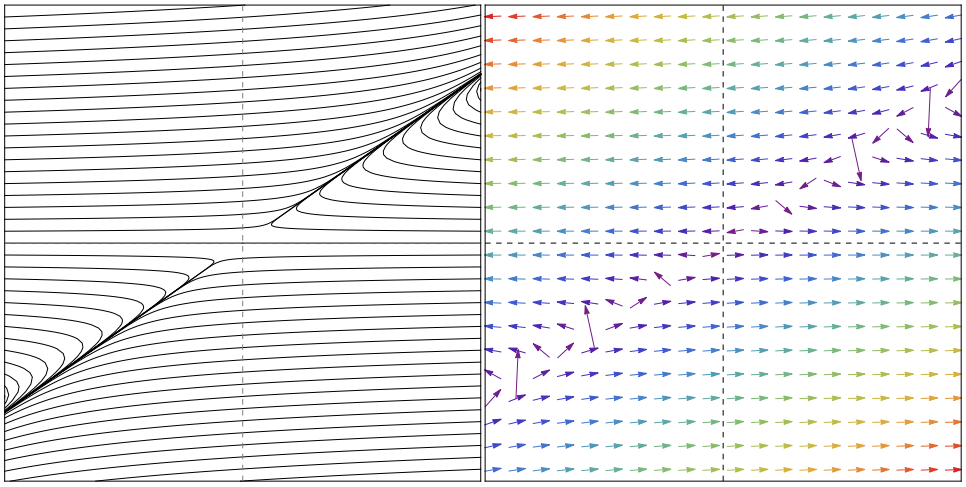

Figure 4.8 Phase portrait in the case of $\gamma = -2.1$, $\omega = 0$ and $\omega_{\mathrm{B}} = -1$ for the fixed point $S = 3$ and $\Omega_{\mathrm{B}} = 0$. The center is the origin and the axes are δS and $\delta\Omega_{\mathrm{B}}$, respectively. It is a saddle point.

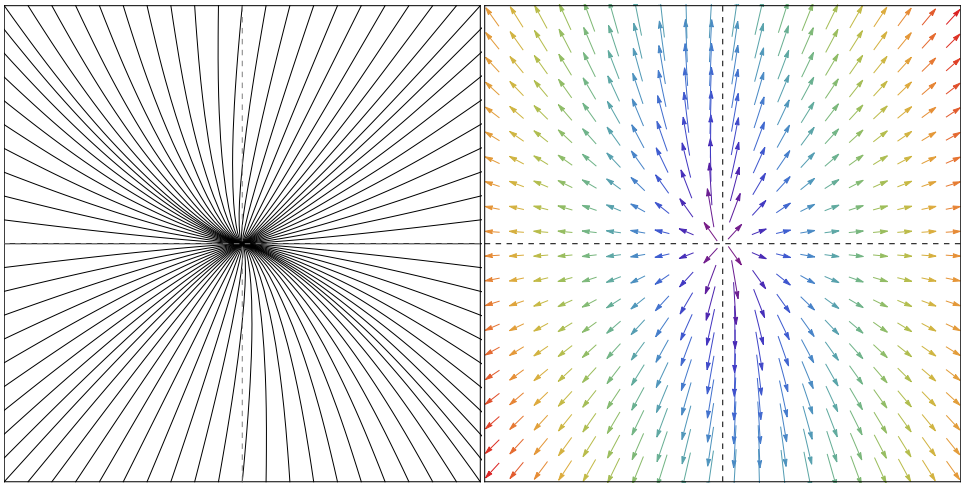

Figure 4.9 Phase portrait in the case of $\gamma = 0.25$, $\omega = 0$ and $\omega_{\mathrm{B}} = -1$ for the fixed point $S = -3$ and $\Omega_{\mathrm{B}} = 0$. The center is the origin and the axes are δS and $\delta\Omega_{\mathrm{B}}$, respectively. This shows a typical behavior of an unstable point.

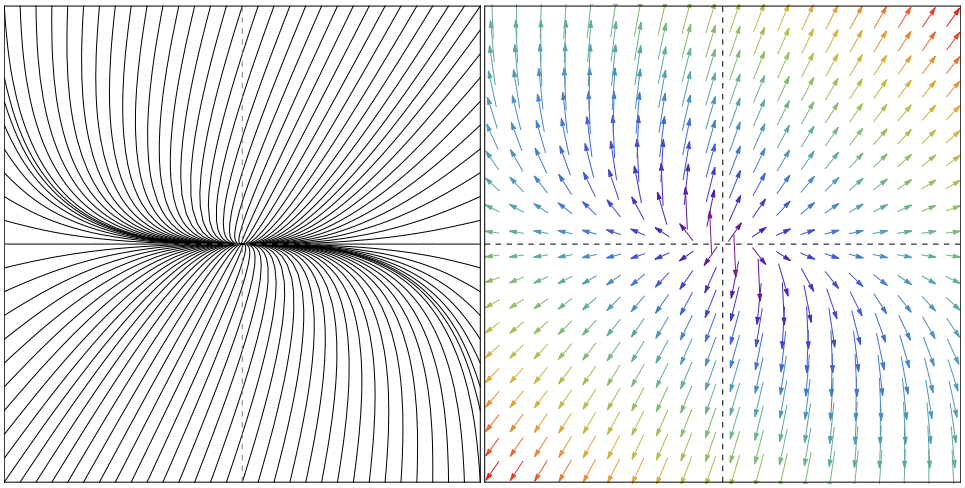

Figure 4.10 Phase portrait in the case of $\gamma = -0.25$, $\omega = 0$ and $\omega_{\mathrm{B}} = -1$ for the fixed point $S = -3$ and $\Omega_{\mathrm{B}} = 0$. The center is the origin and the axes are δS and $\delta\Omega_{\mathrm{B}}$, respectively. This shows a typical behavior of an unstable point as well.

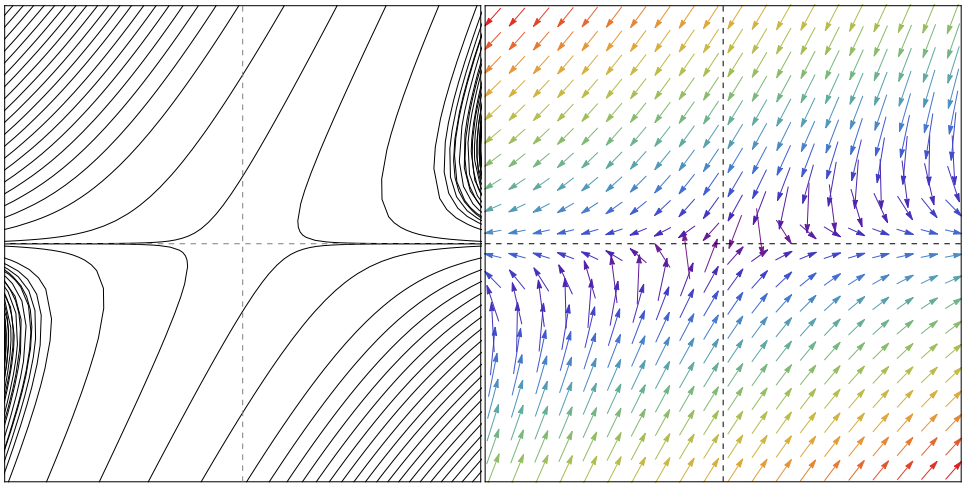

Figure 4.11 Phase portrait in the case of $\gamma = 2$, $\omega = 0$ and $\omega_B = -1$ for the fixed point $S = -3$ and $\Omega_B = 0$. The center is the origin and the axes are δS and $\delta\Omega_B$, respectively. This shows a typical behavior of a saddle point diverging horizontally and converging vertically.

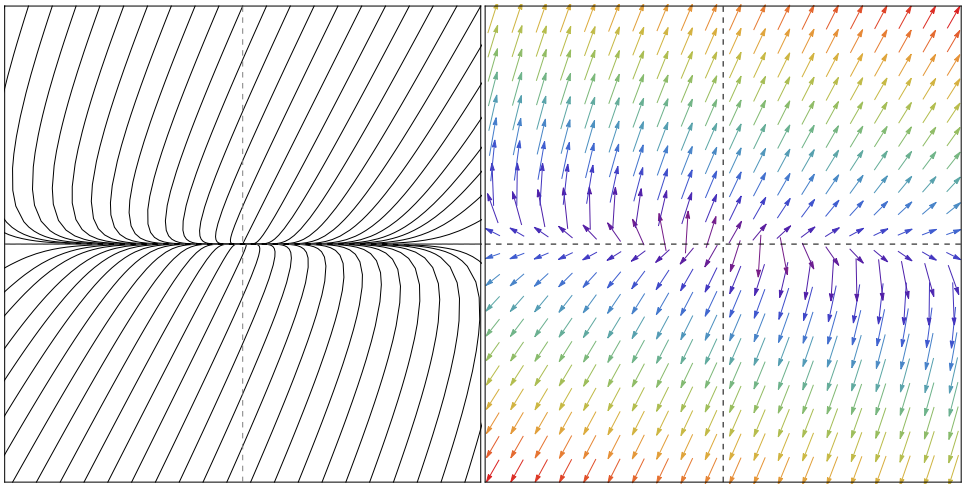

Figure 4.12 Phase portrait in the case of $\gamma = -2$, $\omega = 0$ and $\omega_B = -1$ for the fixed point $S = -3$ and $\Omega_B = 0$. The center is the origin and the axes are δS and $\delta\Omega_B$, respectively. This is an unstable point.

4.1.3 The anisotropic fixed point I

$$\Omega = 0,\ \ \Omega_{\rm B} = \frac{(\omega_{\rm B} - \gamma - 1)(\omega_{\rm B} + 3\gamma - 1)}{(\omega_{\rm B} + \gamma - 1)^2},\ \ S = \frac{6\gamma}{\omega_{\rm B} + \gamma - 1} \tag{4.6}$$

It shows a balanced expansion in different directions. The eigenvalues are

$$\left\{3\left(\omega_{\rm B} + \gamma - \frac{4\gamma^2}{\omega_{\rm B} + \gamma - 1}\right),\ \ \frac{3(\omega_{\rm B} - \gamma - 1)(\omega_{\rm B} + 3\gamma - 1)}{2(\omega_{\rm B} + \gamma - 1)}\right\}$$

For convenience we assume $\omega = 0$ and restrict only $\omega_{\rm B} < \omega$. We have a stable node if either $\omega_{\rm B} + \gamma > 1$ or it satisfies both

$$2\omega_{\rm B} < 1 + 6\gamma \ + \ \sqrt{1 + 16\omega_{\rm B}(\omega_{\rm B} - 1)}$$

and

$$1 + 6\gamma < 2\omega_{\rm B} \ + \ 2\sqrt{1 + 16\omega_{\rm B}(\omega_{\rm B} - 1)}$$

We find a saddle point if either

$$\omega_{\rm B} \leq 1 + \gamma \ \ \wedge \ \ 1 + 6\gamma + \sqrt{1 + 16\omega_{\rm B}(\omega_{\rm B} - 1)} \leq 2\omega_{\rm B}$$

or

$$\omega_{\rm B} + 3\gamma \leq 1 \ \ \wedge \ \ 2\omega_{\rm B} + \sqrt{1 + 16\omega_{\rm B}(\omega_{\rm B} - 1)} \leq 1 + 6\gamma$$

The fixed point becomes unstable if either $1 + \gamma < \omega_{\rm B}$ or

$$3\gamma + \omega_{\rm B} > 1 \ \ \wedge \ \ \gamma + \omega_{\rm B} < 1$$

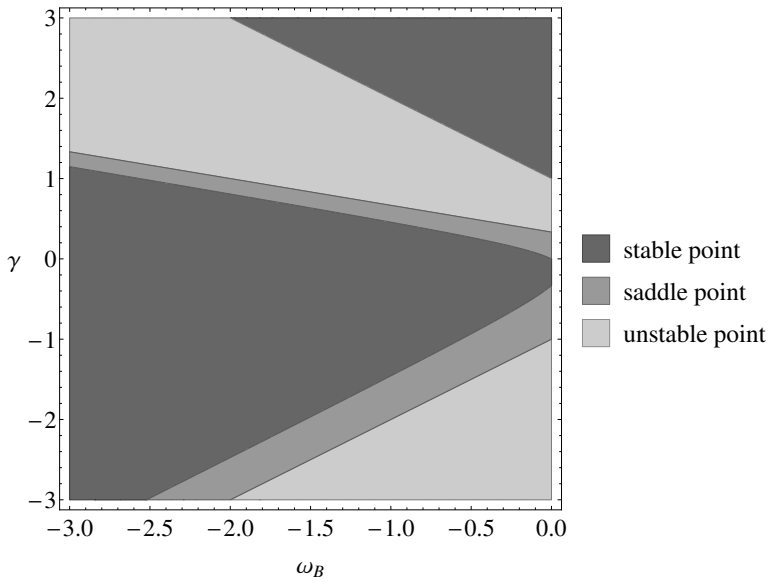

Figure 4.13 Region plot of the anisotropic fixed point 4.1.3. It shows the stability of the fixed point according to dark energy parameter $\omega_{\rm B}$ and γ. x axis is $\omega_{\rm B}$ and y axis is γ. The darkest region represents the range of having a stable point. The second darkest region corresponds to the area of having a saddle point. The brightest region represents the range of having an unstable point.

Since the condition in mathematical description is rather complicated, the region plot gives a better visualization here. The region plot of the anisotropic fixed point 4.1.3 is shown in Fig. 4.13. It shows the stability of the fixed point according to dark energy parameter ω_{B} and γ. ω_{B} is restricted by the assumption $\omega_{\mathrm{B}} < \omega = 0$. If ω_{B} and γ are in the darkest region the fixed point is a stable point. In the gray area (the second darkest one), the fixed point becomes a saddle point. The fixed point is an unstable point in the rest region (the brightest one).

4.1.4 The anisotropic fixed point II

$$\Omega = 0, \quad \Omega_{\mathrm{B}} = -\frac{\omega_{\mathrm{B}} + \gamma}{4\gamma^2}, \quad S = \frac{3(\omega_{\mathrm{B}} + \gamma)}{2\gamma} \tag{4.7}$$

We can find two eigenvalues as below

$$\left\{-\frac{3}{4}\left(1 \pm \frac{\sqrt{\gamma^{14}\left[\,6\gamma^3+\gamma^2(3+2\omega_{\mathrm{B}})+2\gamma(2-3\omega_{\mathrm{B}})\omega_{\mathrm{B}}-2(\omega_{\mathrm{B}}-1)\omega_{\mathrm{B}}^2\,\right]}}{\gamma^8}\right)\right\}$$

Again assuming $\omega_{\mathrm{B}} < 0$, it is a saddle point if either $0 < \omega_{\mathrm{B}} + \gamma < 1$ or

$$\gamma < 0 \quad \wedge \quad 2\omega_{\mathrm{B}} \leq 1 + 6\gamma + \sqrt{1 + 16\omega_{\mathrm{B}}(\omega_{\mathrm{B}} - 1)}$$

or

$$\gamma > 0 \quad \wedge \quad 1 + 6\gamma \leq 2\omega_{\mathrm{B}} + \sqrt{1 + 16\omega_{\mathrm{B}}(\omega_{\mathrm{B}} - 1)}$$

The fixed point becomes a stable point under the certain condition as well. However the stability condition for this fixed point is too long so it is not written here, but is shown in Fig. 4.14. It shows the stability of the fixed point according to dark energy parameter ω_{B} and γ. In the given assumptions, the fixed point is an attractor when ω_{B} and γ stay in the darker region. The fixed point become a saddle point when they are in the brighter area.

Note that when $\omega_{\mathrm{B}} + \gamma > 0$, Ω_{B} becomes negative. A fixed point does not exist physically for parameter values which would result in negative energy densities.

4.1.5 The scaling solution

$$\begin{aligned} \Omega &= \frac{3\gamma^2 + \gamma(1 + \omega - 2\omega_{\mathrm{B}}) + (\omega - \omega_{\mathrm{B}})(\omega_{\mathrm{B}} - 1)}{4\gamma^2}, \\ \Omega_{\mathrm{B}} &= \frac{(1-\omega)(\omega - \omega_{\mathrm{B}} - \gamma)}{4\gamma^2}, \quad S = \frac{3(\omega_{\mathrm{B}} - \omega + \gamma)}{2\gamma} \end{aligned} \tag{4.8}$$

It is a physically distinct fixed point from the former, since the universe has matter. When $0 < \Omega < 1$ we have a scaling solution since the matter energy density scales

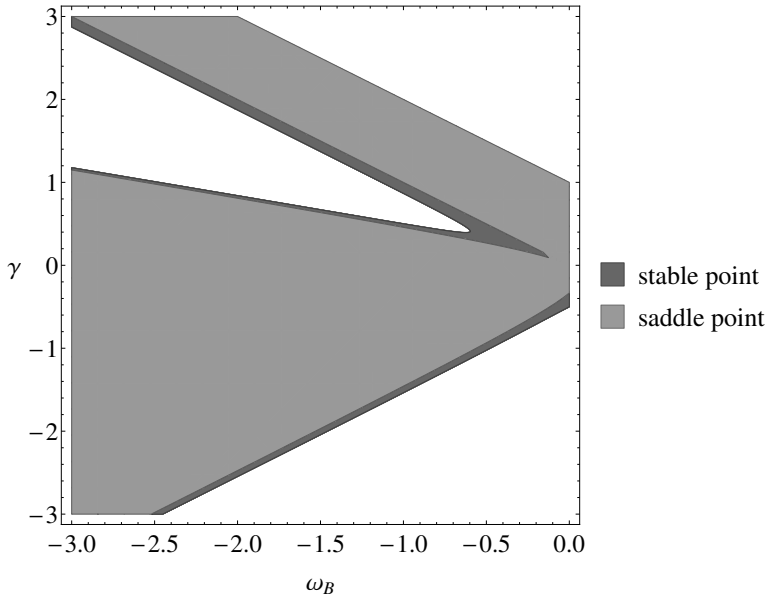

Figure 4.14 Region plot of the anisotropic fixed point 4.1.4. It shows the stability of the fixed point according to dark energy parameter $\omega_{\rm B}$ and γ. x axis is $\omega_{\rm B}$ and y axis is γ. The darker region represents the range of having a stable point. The brighter region represents the range of having a saddle point.

with the other components so that their relative amount is kept constant. We can find two eigenvalues from the fixed point as below

$$\left\{\frac{3}{4}\left(\omega - 1 \pm \frac{\omega_*}{\gamma^3}\right)\right\}$$

where

$$\begin{aligned}\omega_*^2 \equiv\ & \gamma^4(1-\omega)\left[6\gamma^3 - \gamma^2(5\omega - 2\omega_{\rm B} - 3)\right. \\ & \left. -2\gamma(\omega - 3\omega_{\rm B} + 2)(\omega - \omega_{\rm B}) - 2(\omega - \omega_{\rm B})^2(\omega_{\rm B} - 1)\right]\end{aligned}$$

However the assumption $\omega_{\rm B} < \omega = 0$ makes it exactly the same as a fixed point (4.7) for S and $\Omega_{\rm B}$. It turns out to have exactly the same stability conditions as well in this limit. Here we present the perturbation equations of this fixed point without assumptions for parameters :

$$\begin{aligned}B_1 &= -\frac{3(1-\omega)(\gamma^2 + 2\gamma(\omega - \omega_{\rm B}) - (\omega - \omega_{\rm B})^2)}{4\gamma^2}, \\ B_2 &= -\frac{9(\gamma + \omega - \omega_{\rm B})(3\gamma - \omega + \omega_{\rm B})}{4\gamma}, \\ B_3 &= -\frac{(1-\omega)(2\gamma^2 + \gamma(1-\omega) - (1-\omega)(\omega - \omega_{\rm B}))(\gamma - \omega + \omega_{\rm B})}{4\gamma^3}, \\ B_4 &= -\frac{3(1-\omega)(\gamma - \omega + \omega_{\rm B})^2}{4\gamma^2}\end{aligned}$$

where B_1, B_2, B_3 and B_4 are the coefficients of the perturbed terms of δS and $\delta\Omega_{\rm B}$ as defined in (3.36). If we assume $\omega = 0$, then these reduce to the coefficients of the perturbed terms in former fixed point exactly.

4.2 Numerical solutions

Now we can compare our analytical considerations with the numerical computations. Since our two evolution equations (3.26) and (3.28) are the ordinary differential equations, it can be solved for time. In order to solve this, the initial conditions are needed. We can study the relevant solutions for the dark energy problem by setting a dust-dominated universe, $\omega = 0$ as our initial condition. The results only depend on dark energy properties, $\omega_{\rm B}$ and γ.

The phase portrait in the case of $\gamma = 0.25$ and $\omega_{\rm B} = -1$ is shown in Fig. 4.15. The solution (4.2) is shown at the origin. Trajectories converge towards the origin horizontally, but diverge vertically which make it a saddle point as expected. The solution (4.3) is an unstable point, which is at $(\pm 3, 0)$. Trajectories starting around this fixed point move away from the starting point. The solution (4.6) is a stable point as expected from the stability condition. The calculated value of (4.6) is $(-0.857, 0.918)$ which attracts trajectories from everywhere. This figure agrees completely with the analysis of each fixed point, Figure 4.1, 4.5 and 4.9.

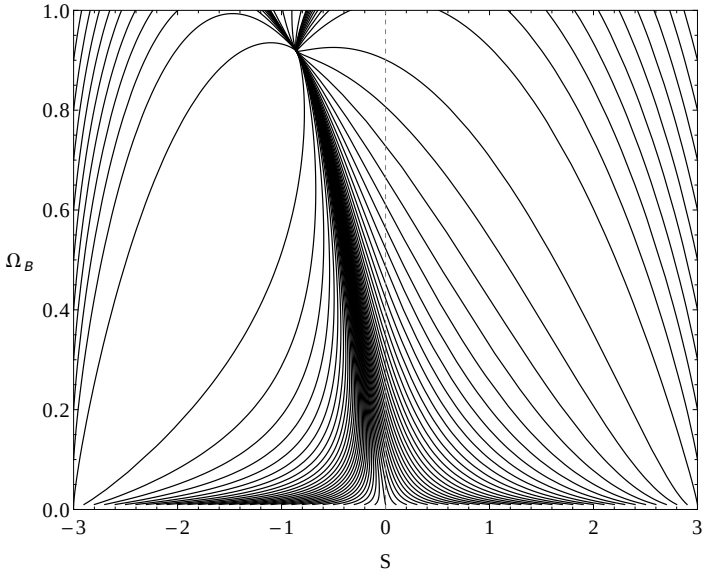

Figure 4.15 Phase portrait in the case of $\gamma = 0.25$ and $\omega_{\rm B} = -1$. The axes are S and $\Omega_{\rm B}$, respectively.

The phase portrait in the case of $\gamma = -0.25$ and $\omega_{\rm B} = -1$ is shown in Fig. 4.16. It shows mostly similar behavior for the solutions (4.2), (4.3) and (4.6). The calculated value of (4.6) is $(0.666, 0.951)$. This figure agrees completely with the analysis of each fixed point, Figure 4.2, 4.6 and 4.10.

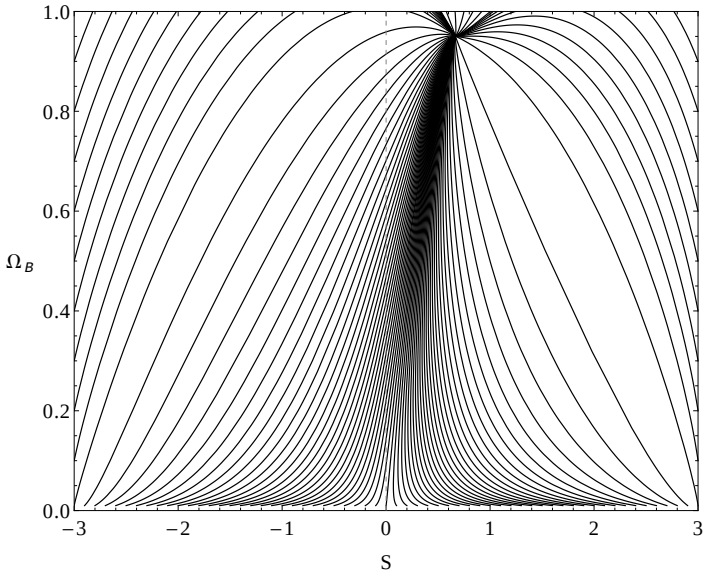

Figure 4.16 Phase portrait in the case of $\gamma = -0.25$ and $\omega_{\rm B} = -1$. The axes are S and $\Omega_{\rm B}$, respectively.

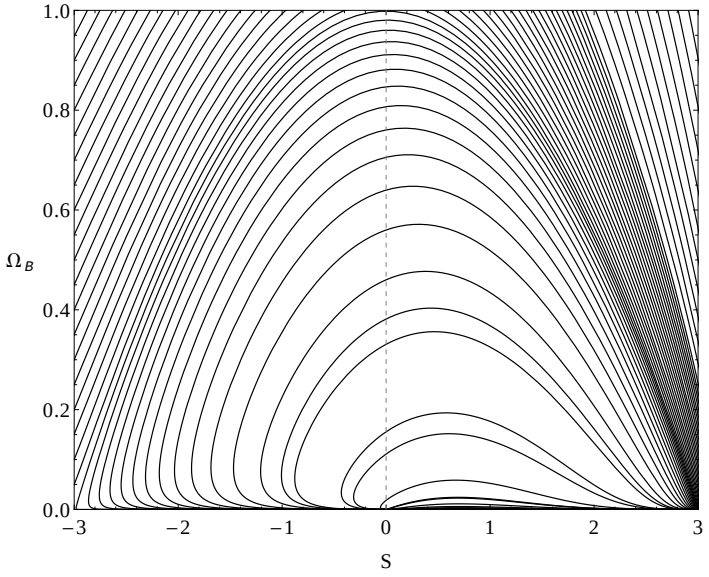

Figure 4.17 Phase portrait in the case of $\gamma = 2$ and $\omega_{\rm B} = -1$. The axes are S and $\Omega_{\rm B}$, respectively. This is a scaling solution.

The phase portrait in the case of $\gamma = 2$ and $\omega_{\rm B} = -1$ is shown in Fig. 4.17. This is a scaling solution. Trajectories starting from the one of the solution (4.3) at $(3, 0)$ all go towards the origin which proves that it is an unstable point. The origin, solution of (4.2) is stable point. The other fixed point of (4.3) at $(-3, 0)$ is a saddle point. Trajectories starting from the positive numbers of bottom curve to the origin. This figure agrees completely with the analysis of each fixed point, Figure 4.3, 4.7 and 4.11 as well.

The phase portrait in the case of $\gamma = -2$ and $\omega_{\rm B} = -1$ is shown in Fig. 4.18. It can be easily checked that all trajectories from the bottom converge to the certain point. The solution of (4.2) is a saddle point converging horizontally and diverging vertically. One of the solution (4.3) at $(3, 0)$ is another saddle point. Trajectories beginning from the bottom at the left side of this point move to left, on the other hand trajectories coming down from the top at the right side slide to right. The other solution of (4.3) at $(-3, 0)$ an unstable point. The solution of (4.7) shows very interesting behavior. In this case, the eigenvalues of (4.7) are complex conjugates. According to the stability condition, the sign of the real part determines a behavior. Here it is negative and it is an attractor. The calculated value of (4.7) is $(2.25, 0.188)$. This figure agrees completely with the analysis of each fixed point, Figure 4.4, 4.8 and 4.12 as well.

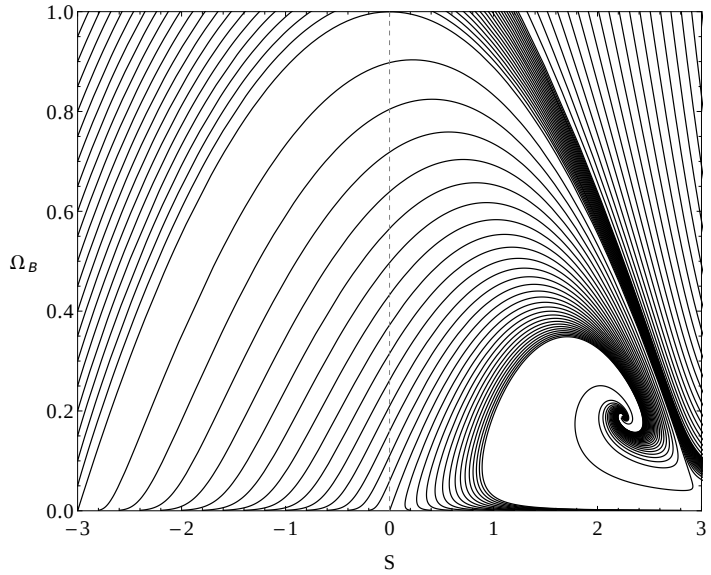

Figure 4.18 Phase portrait in the case of $\gamma = -2$ and $\omega_{\rm B} = -1$. The axes are S and $\Omega_{\rm B}$, respectively.

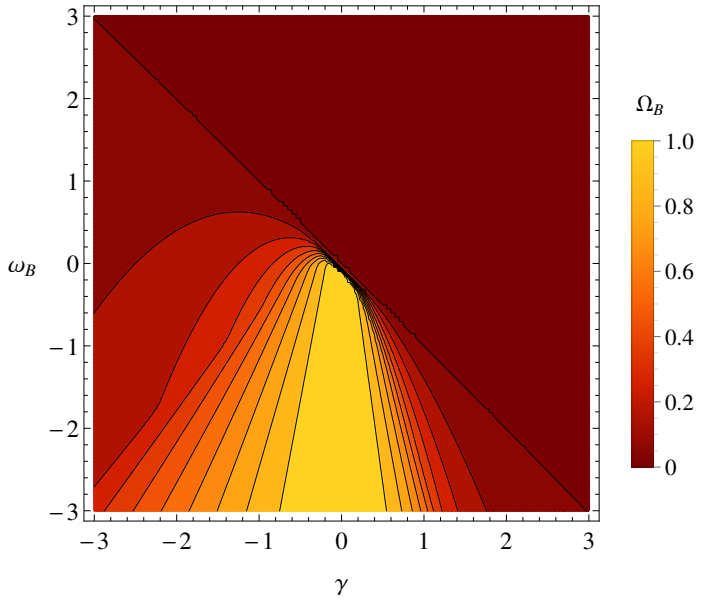

Figure 4.19 Contour plot of Ω_{B} according to ω_{B} and γ in a flat universe. It represents the asymptotic state of dark energy in the universe starting from a matter-dominated state. The axes are γ and ω_{B}, respectively. The contour represents the value of the dark energy density paramter Ω_{B}.

The contour plot of Ω_{B} according to ω_{B} and γ in a flat universe is shown in Fig. 4.19. It represents the asymptotic state of dark energy in the universe starting from a matter-dominated state. The future is determined by the dark energy parameters ω_{B} and γ. The contour represents the value of the dark energy density paramter Ω_{B}. The darkest area (red area) corresponds to an isotropically expanding matter-dominated universe, since there is no dark energy in that universe eventually, it will be matter-dominated forever. The brightest area (yellow area) represents when there is no matter in it. Therefore the universe is dominated by dark energy and expands anisotropically forever when $\Omega_{\mathrm{B}} = 1$. Otherwise it exhibits a scaling model between $0 < \Omega_{\mathrm{B}} < 1$.

The contour plot of Ω according to ω_{B} and γ is shown in Fig. 4.20. Note that Ω here does not mean the total energy density of the universe. As it has been used so far, it is a parameter of dark matter (perfect fluid). It shows the asymptotic state of dark matter in the universe. FRLW universe is used as an initial condition. Even though the sum of Ω and Ω_{B} does not become simply one due to the presence of shear S, mostly overall figure shows the opposite state of Ω_{B}.

The contour plot of shear S according to ω_{B} and γ is shown in Fig. 4.21. It describes the asymptotic state of shear in the universe starting from a matter-dominated state. The red area of Figure 4.19 and the yellow area of Figure 4.20

corresponding to $\gamma+\omega_{\mathrm{B}} > 0$ in this plot means isotropization, $S = 0$. The possible range of shear S is obtained from the generalized Friedmann equation (3.23).

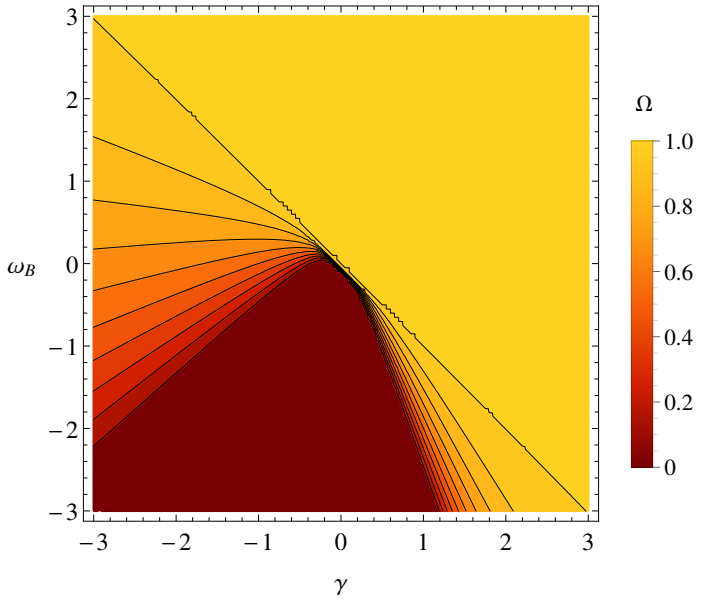

Figure 4.20 Contour plot of Ω according to ω_{B} and γ. The axes are γ and ω_{B}, respectively. The contour represents the value of the dark energy density paramter Ω.

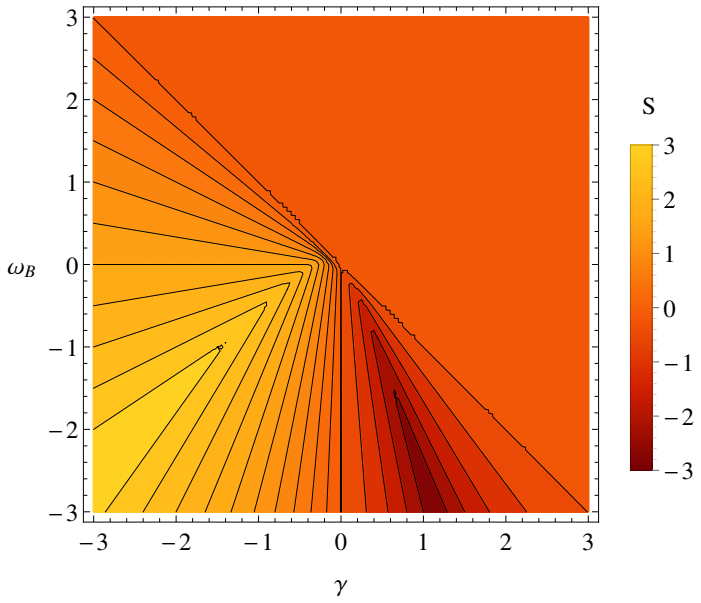

Figure 4.21 Contour plot of shear S according to ω_{B} and γ. It describes the asymptotic state of shear in the universe starting from a matter-dominated state. The axes are γ and ω_{B}, respectively. The contour represents the value of the dark energy density paramter S.

Chapter 5

Fixed points in a curved geometry

5.1 Analytical stability analysis

Let us finally include curvature in the system. There has been various ideas about the possibility that the present horizontal scale can be related to the anisotropies. Also, if anisotropy and the curvature have a common cosmological origin with accelerating expansion of the universe, it will explain the possible properties of dark energy (Koivisto et al. 2011). Here, we consider a curved geometry with a preferred axis which is classified into two cases. When k is positive, we have the Kantowski-Sachs metric

$$ds^2 = -dt^2 + b^2(t)dy^2 + a^2(t)\left[d\xi^2 + \frac{1}{|k|}\sin^2(|k|^{\frac{1}{2}}\xi)d\phi^2\right] \tag{5.1}$$

and when k is negative, we have the Bianchi III metric

$$ds^2 = -dt^2 + b^2(t)dy^2 + a^2(t)\left[d\xi^2 + \frac{1}{|k|}\sinh^2(|k|^{\frac{1}{2}}\xi)d\phi^2\right] \tag{5.2}$$

To find a fixed point for a curved geometry mostly similar computations are conducted as a flat case. However due to the presence of a curvature we have a perturbation equation for K

$$K = K_0 + \delta K \tag{5.3}$$

where K_0 is the background value which is our fixed point. Also we have an additional assumption $K' = \delta K' = 0$. In the process of getting rid of Ω by using Friedmann equation, Ω is needed to be newly defined from (3.33)

$$\Omega = 1 - \Omega_{\mathrm{B}} - \frac{1}{9}S^2 - \frac{1}{3}K \tag{5.4}$$

Then new perturbation equations are expanded to first order as it is done before

$$\begin{aligned}\delta S' &= C_1\,\delta S + C_2\,\delta\Omega_{\rm B} + C_3\,\delta K\\ \delta\Omega_{\rm B}' &= C_4\,\delta S + C_5\,\delta\Omega_{\rm B} + C_6\,\delta K\\ \delta K' &= C_7\,\delta S + C_8\,\delta\Omega_{\rm B} + C_9\,\delta K\end{aligned} \tag{5.5}$$

which can be written in a matrix form :

$$\begin{pmatrix}\delta S'\\ \delta\Omega_{\rm B}'\\ \delta K'\end{pmatrix} = \begin{pmatrix}C_1 & C_2 & C_3\\ C_4 & C_5 & C_6\\ C_7 & C_8 & C_9\end{pmatrix}\begin{pmatrix}\delta S\\ \delta\Omega_{\rm B}\\ \delta K\end{pmatrix} \tag{5.6}$$

Now we can find the eigenvalues from the characteristic euqation to figure out how fixed points behavior under the perturbations. Our system with curvature turns out to have 3 fixed points.

5.1.1 An anisotropically expanding empty universe

$$\Omega = 0, \quad \Omega_{\rm B} = 0, \quad S = \frac{3}{2}, \quad K = -\frac{9}{4} \tag{5.7}$$

There is neither perfect nor imperfect fluid in this universe. With curvature parameter K we can find three eigenvalues as follow

$$\left\{-\frac{3}{2},\ -3\omega,\ -3\omega_{\rm B}\right\}$$

The solution is a stable node if both $\omega > 0$ and $\omega_{\rm B} > 0$, otherwise it is a saddle point.

5.1.2 An anisotropically expanding matter-dominated universe

$$\Omega = -3\omega, \quad \Omega_{\rm B} = 0, \quad S = \frac{3}{2}(1+3\omega), \quad K = -\frac{9}{4}(1-\omega)(1+3\omega) \tag{5.8}$$

We have three eigenvalues

$$\left\{3(\omega + 3\gamma\omega - \omega_{\rm B}),\ \ -\frac{3}{4}\left(1-\omega \pm \sqrt{(1-\omega)(1+7\omega+24\omega^2)}\right)\right\}$$

If $\omega = -1/3$, density parameter for matter Ω becomes unity and all other variables become zero. In that case, this recovers FLRW universe (4.2). If $\omega = 0$, this becomes exactly the same as the previous empty universe case (5.7). Generally the solution becomes a stable node if

$$-\frac{1}{3} < \omega < 0 \quad \wedge \quad \gamma > \frac{\omega_{\rm B} - \omega}{3\omega}$$

otherwise it is a saddle point except for when

$$\omega > 1 \quad \wedge \quad \gamma \neq \frac{\omega_{\rm B} - \omega}{3\omega}$$

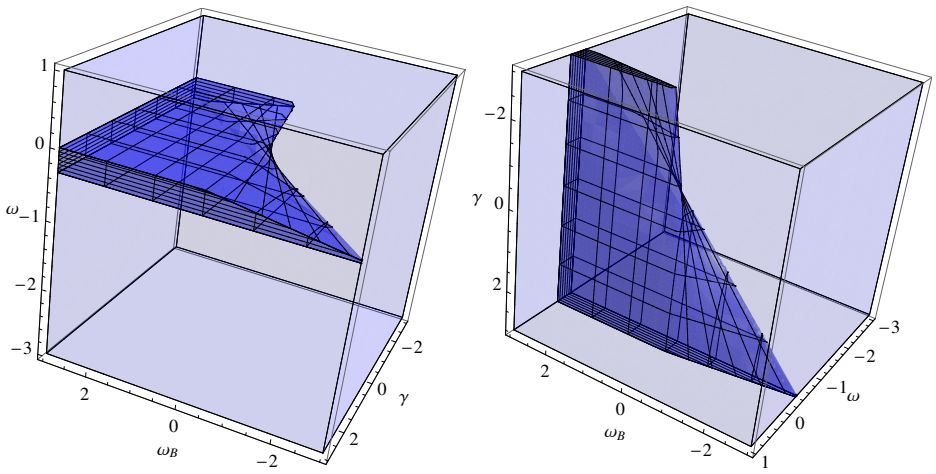

Figure 5.1 3D region plot of the fixed point 5.1.2. The mesh region in the box represents a stable region. If $\omega, \omega_{\rm B}$ and γ have values in this region, the fixed point becomes an attractor. If they have values outside the mesh region, but still remain in the box, then the solution becomes a saddle point. The box does not include the region where $\omega > 1$.

5.1.3 The anisotropic fixed point

$$\begin{aligned}
\Omega &= 0, \\
\Omega_{\rm B} &= -\frac{3\omega_{\rm B}}{(1+3\gamma)^2}, \\
S &= \frac{3(1+3\gamma+3\omega_{\rm B})}{2(1+3\gamma)}, \\
K &= \frac{9(3\omega_{\rm B}^2 + 2\omega_{\rm B}(3\gamma-1) - (1+3\gamma)^2)}{4(1+3\gamma)^2}
\end{aligned} \tag{5.9}$$

We find three eigenvalues as below

$$\left\{ \frac{3\omega_{\rm B}}{1+3\gamma} - 3\omega \, , \;\; \frac{3}{4}\left(\frac{\omega_{\rm B} \pm \gamma_*}{1+3\gamma} - 1 \right) \right\}$$

where

$$\gamma_*^2 \equiv (1+3\gamma)^2 + 6(1+3\gamma)(1+4\gamma)\omega_{\rm B} + (17-48\gamma)\omega_{\rm B}^2 - 24\omega_{\rm B}^3$$

Recall the physical requirement of positive energy density parameters. The parameter region for which $\Omega_B < 0$ is probably not physically consistent. A general

stability solution for this fixed point is very complicated. Here we look at the following conditions of our interest.

(a) First we assume $\omega = 0$ and restrict only $\omega_{\rm B} < \omega$ as before. Then the solution becomes a stable node if both

$$\omega_{\rm B} + 2\sqrt{(\omega_{\rm B} - 1)\omega_{\rm B}} < 1 + 3\gamma$$

and

$$\omega_{\rm B} \geq -\frac{1}{8} \quad || \quad 1 + 3\gamma \ \leq \ \omega_{\rm B} + 4\sqrt{2}\,|\omega_{\rm B}|\sqrt{\frac{\omega_{\rm B} - 1}{8\omega_{\rm B} - 1}}$$

It is a saddle point if either

$$0 < 1 + 3\gamma \ \leq \ \omega_{\rm B} + 2\sqrt{(\omega_B - 1)\omega_{\rm B}}$$

or at the same time if it satisfies both $1 + 3\gamma < 0$ and

$$\omega_{\rm B} \geq -\frac{1}{8} \quad || \quad \omega_{\rm B} - 4\sqrt{2}\,|\omega_{\rm B}|\sqrt{\frac{\omega_{\rm B} - 1}{8\omega_{\rm B} - 1}} \leq 1 + 3\gamma$$

The region plot of the anisotropic fixed point (a) is shown in Fig. 5.2. It shows the stability of the fixed point according to dark energy parameter $\omega_{\rm B}$ and γ. In the given assumptions, the fixed point is an attractor when $\omega_{\rm B}$ and γ have values in the darker region. The fixed point becomes a saddle point when they have values in the brighter region.

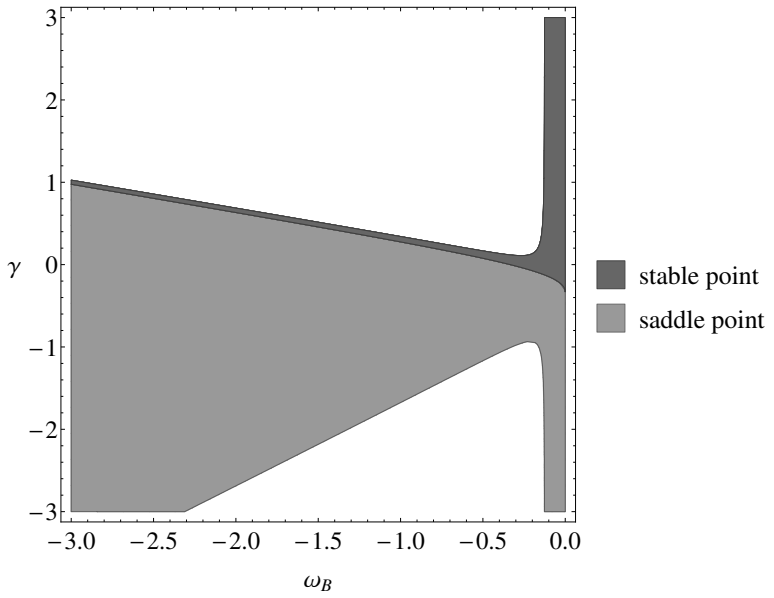

Figure 5.2 Region plot of the anisotropic fixed point (a). It shows the stability of the fixed point according to dark energy parameter $\omega_{\rm B}$ and γ. x axis is $\omega_{\rm B}$ and y axis is γ. The darker region represents the range of having a stable point. The brighter region represents the range of having a saddle point.

(b) The second interesting case is found by assuming $\omega = 1/3$ and $\omega_{\rm B} < \omega$. In that case, we have an attractor if either ① or ② or ③.

① if both $\omega_{\rm B} < -1/8$ and

$$1 + 3\gamma + 2\sqrt{(\omega_{\rm B} - 1)\omega_{\rm B}} < \omega_{\rm B} \leq 1 + 3\gamma + 4\sqrt{2}\,|\omega_{\rm B}|\sqrt{\frac{\omega_{\rm B} - 1}{8\omega_{\rm B} - 1}}$$

② if $\omega_{\rm B} + 2\sqrt{(\omega_{\rm B} - 1)\omega_{\rm B}} < 1 + 3\gamma \leq \omega_{\rm B} + 4\sqrt{2}\,|\omega_{\rm B}|\sqrt{\frac{\omega_{\rm B} - 1}{8\omega_{\rm B} - 1}}$

③ if both $-1/8 \leq \omega_{\rm B} < 0$ and

$$1 + 3\gamma + 2\sqrt{(\omega_{\rm B} - 1)\omega_{\rm B}} < \omega_{\rm B} \quad || \quad \omega_{\rm B} + 2\sqrt{(\omega_{\rm B} - 1)\omega_{\rm B}} < 1 + 3\gamma$$

The solution is a saddle point if either ① or ② or ③.

① if both $\omega_{\rm B} < 0$ and

$$1 + 3\gamma + 2\sqrt{(\omega_{\rm B} - 1)\omega_{\rm B}} \leq \omega_{\rm B} \quad \wedge \quad \gamma < -\frac{1}{3}$$

② if both $\omega_{\rm B} < 0$ and

$$-\frac{1}{3} < \gamma < \frac{1}{3}\left(\omega_{\rm B} - 1 + 2\sqrt{(\omega_{\rm B} - 1)\omega_{\rm B}}\right)$$

③ if both $0 \leq \omega_{\rm B} < 1/3$ and $1 + 3\gamma \neq 0$.

The region plot of the anisotropic fixed point (b) is shown in Fig. 5.3. It shows the stability of the fixed point according to dark energy properties $\omega_{\rm B}$ and γ. In the given assumption, the fixed point is a stable point when $\omega_{\rm B}$ and γ stay in the darker region. The fixed point become a saddle point when they are in the brighter region.

(c) Next, we look at the cases of $\omega_{\rm B} + \gamma = -1/3$ and $\omega_{\rm B} < \omega$.
The solution is a stable node if $\omega > -1/3$ and $\omega_{\rm B} \geq -1/2$.
It is a saddle point if at least one of the conditions ① - ④ given below is true.

① if both $\omega < -1/3$ and $\omega_{\rm B} \geq -1/2$

② if $\omega = -1/3$

③ if both $\omega \leq 0$ and $\omega_{\rm B} \geq -1/3$

④ if both $\omega > 0$ and

$$-\frac{1}{3} \leq \omega_{\rm B} < 0 \quad || \quad \omega_{\rm B} > 0$$

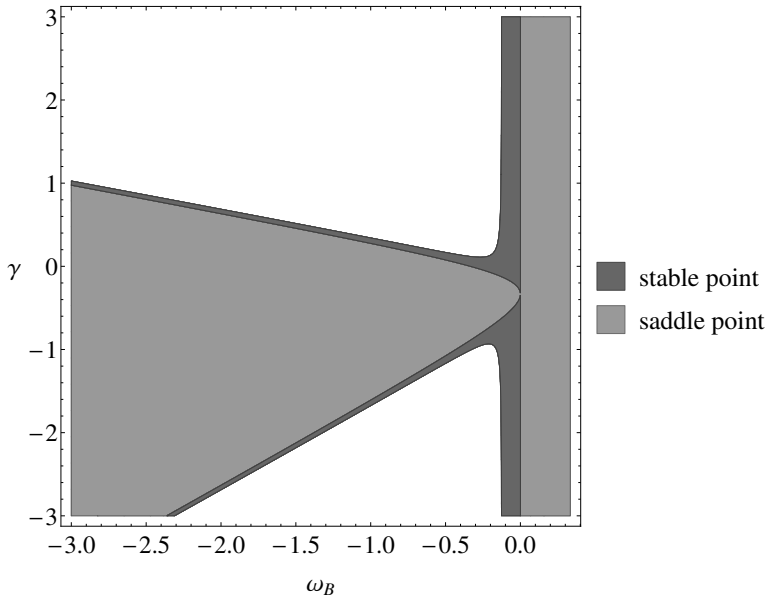

Figure 5.3 Region plot of the anisotropic fixed point (b). It shows the stability of the fixed point according to dark energy properties $\omega_{\rm B}$ and γ. x axis is $\omega_{\rm B}$ and y axis is γ. The darker region represents the range of having a stable point. The brighter region represents the range of having a saddle point.

This solution corresponds to a shear-free condition. In this case, the matter stresses cancel the effect of anisotropic curvature as a generator of the shear. Such models thus allow significantly larger anisotropies, which however can be constrained by the anisotropic modulation of the distance measurements, such as the directional dependence of the luminosity-distance relation that can be probed by the supernovae Ia light curves (Koivisto et al. 2011). These models thus provide an interesting alternative to the usual Friedmann-Robertson-Walker cosmology. Here, we can take a look at the issue of the stability of the shear-free condition. In realistic models, in addition to the anisotropically stressed fluid that supports the shear-free condition, there would also be usual isotropic matter source.

The region plot of the anisotropic fixed point (c) is shown in Fig. 5.4. It shows the stability of the fixed point according to the equation of state parameters $\omega_{\rm B}$ and ω. In the given assumption, the fixed point is a stable point when $\omega_{\rm B}$ and ω stay in the darker region. The fixed point become a saddle point when they are in the brighter region.

(d) More specifically, we assume $\omega_{\rm B} = -1/3$ and $\omega_{\rm B} < \omega$.
The fixed point is a stable node if either ① or ② or ③.

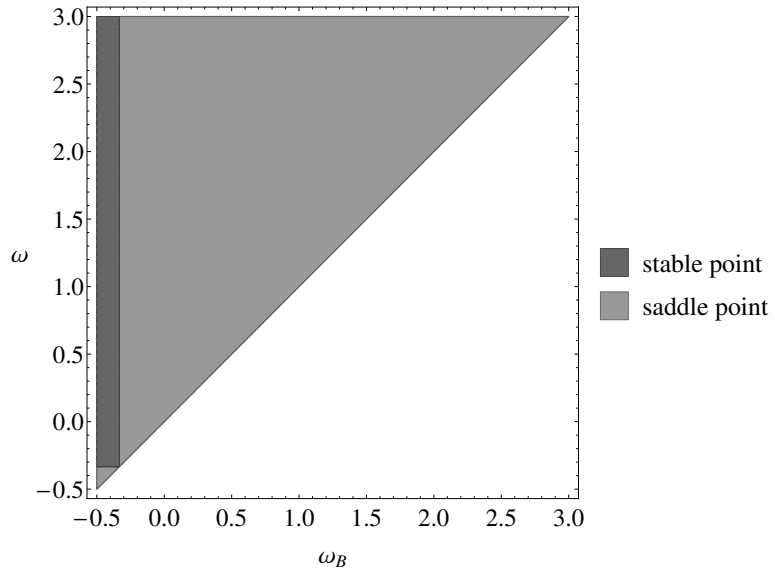

Figure 5.4 Region plot of the anisotropic fixed point (c). Here ω and ω_{B} are the axes. In the given assumptions, the fixed point is an attractor when ω and ω_{B} have values in the darker region. The fixed point becomes a saddle point when they have values in the brighter region.

① if both $9\gamma + 1/\omega + 3 < 0$ and at the same time if either

$$\gamma > 0 \quad \wedge \quad -\frac{1}{3} < \omega \leq -\frac{8\sqrt{10}+5}{123}$$

or

$$\gamma \geq -\frac{4(2\sqrt{10}+5)}{45} \quad \wedge \quad \frac{8\sqrt{10}-5}{123} < \omega \leq \frac{1}{5}$$

② if both $\gamma > 0$ and

$$\gamma \leq -\frac{4(2\sqrt{10}+5)}{45} \quad \wedge \quad \omega > -\frac{8\sqrt{10}+5}{123}$$

③ if both $\omega > 1/5$ and

$$-\frac{4(2\sqrt{10}+5)}{45} \leq \gamma < -\frac{8}{9}$$

The fixed point is a saddle point if either ① or ② or ③.

① if both $9\gamma + 1/\omega + 3 = 0$ and at the same time if either

$$\omega < 0 \quad \wedge \quad \omega \geq -\frac{8\sqrt{10}+5}{123}$$

or

$$\omega > 0 \quad \wedge \quad \omega < \frac{8\sqrt{10}-5}{123}$$

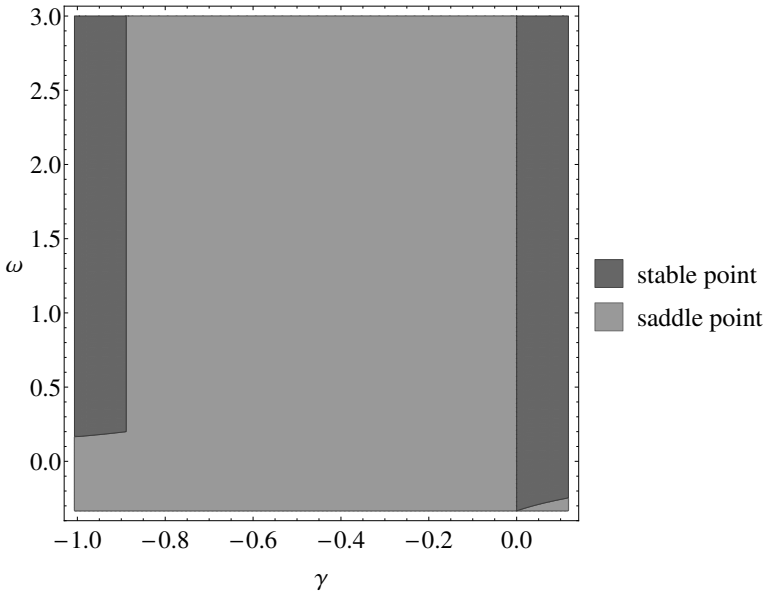

Figure 5.5 Region plot of the anisotropic fixed point (d). Here γ and ω are the axes. In the given assumptions, the fixed point is an attractor when γ and ω have values in the darker region. The fixed point becomes a saddle point when they have values in the brighter region.

② if both $3\omega + 1 > 0$ and at the same time if either $-1/3 < \gamma \leq 0$ or

$$9\gamma + \frac{1}{\omega} + 3 \geq 0 \quad \wedge \quad \omega < -\frac{8\sqrt{10}+5}{123} \quad \wedge \quad \gamma \leq \frac{4(2\sqrt{10}-5)}{45}$$

or

$$\omega < \frac{8\sqrt{10}-5}{123} \quad \wedge \quad -\frac{4(2\sqrt{10}+5)}{45} \leq \gamma < -\frac{1}{3}$$

③ if both $3\gamma + 1 < 0$ and at the same time if either

$$\omega > \frac{1}{5} \quad \wedge \quad \gamma \geq -\frac{8}{9}$$

or

$$9\gamma + \frac{1}{\omega} + 3 \geq 0 \quad \wedge \quad \frac{8\sqrt{10}-5}{123} \leq \omega \leq \frac{1}{5}$$

The region plot of the anisotropic fixed point (d) is shown in Fig. 5.5. It shows the stability of the fixed point according to ω and γ. In the given assumption, the fixed point is a stable point when ω and γ stay in the darker region. The fixed point becomes a saddle point when they are in the brighter region.

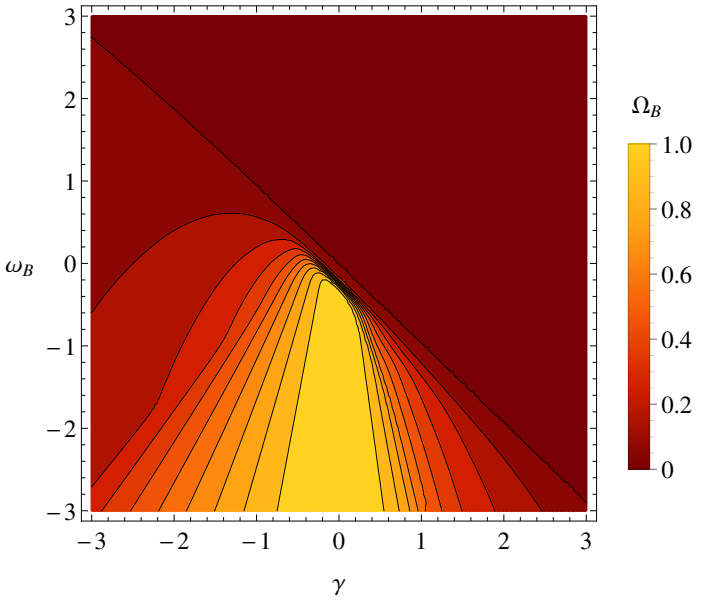

Figure 5.6 Contour plot of dark energy density Ω_{B} according to ω_{B} and γ in a curved universe. It represents the asymptotic state of dark energy in the universe starting from a matter-dominated state. The axes are γ and ω_{B}, respectively. The contour represents the value of the dark energy density paramter Ω_{B}.

5.2 Numerical solutions

Now we can compare our analytical considerations with the numerical computations. Since our three evolution equations (3.26), (3.28) and (3.29) are the ordinary differential equations, it can be solved for time. In order to solve this, the initial conditions are needed. We can study the relevant solutions for the dark energy problem by setting a dust-dominated universe, $\omega = 0$ as our initial condition. The results only depend on dark energy properties, ω_{B} and γ.

The contour plot of dark energy density Ω_{B} according to ω_{B} and γ in a curved universe is shown in Fig. 5.6. It represents the asymptotic state of dark energy in the universe starting from a matter-domiated state. Therefore the future is determined by the dark energy parameters ω_{B} and γ. The contour represents the value of the dark energy density paramter Ω_{B}. The darkest area (red area) corresponds to an isotropically expanding matter-dominated universe, since there is no dark energy in that universe eventually, it will be matter-dominated forever. The brightest area (yellow area) represents when there is no matter in it. Therefore the universe is dominated by dark energy and expands anisotropically forever when $\Omega_{\mathrm{B}} = 1$. Otherwise it exhibits a scaling model between $0 < \Omega_{\mathrm{B}} < 1$. Generally it shows a similar behavior with a flat case.

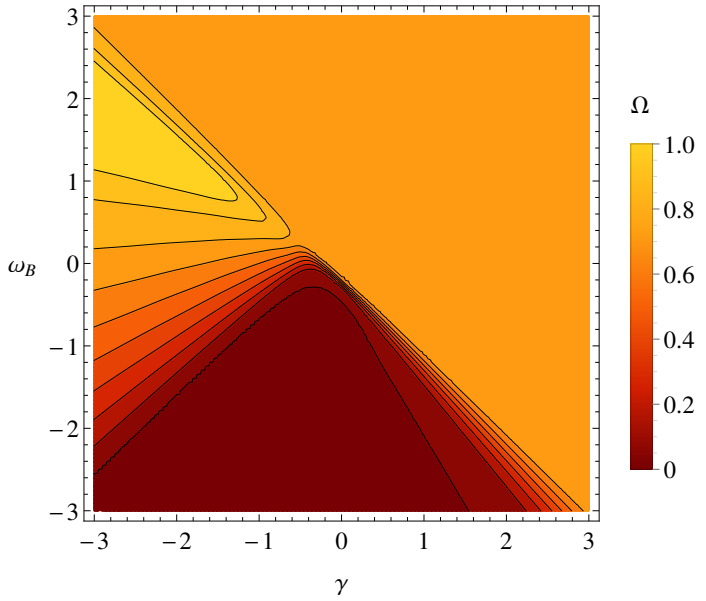

Figure 5.7 Contour plot of dark matter density Ω according to ω_{B} and γ in a curved universe. It represents the asymptotic state of dark matter density in the universe starting from a matter-dominated state. The axes are γ and ω_{B}, respectively. The contour represents the value of the dark matter density paramter Ω.

The contour plot of dark matter density parameter Ω according to ω_{B} and γ in a curved universe is shown in Fig. 5.7. FRLW universe is used as an initial condition as well. Generally it shows a similar behavior with a flat case.

The contour plot of shear S according to ω_{B} and γ in a curved universe is shown in Fig. 5.8. FRLW universe is used as an initial condition as well. The possible range of shear S is obtained from the generalized Friedmann equation (3.23). Generally it shows a similar behavior with a flat case.

Figures 5.9 and 5.10 depict the variation of density parameters versus cosmic time t as example cases [1]. For better comparison shear S and curvature K terms can be transformed as a form of density parameter by making use of the generalized Friedmann equation in 3.23. The generalized Friedmann equation can be rewritten as

$$\Omega + \Omega_{\mathrm{B}} + \frac{1}{9}S^2 + \frac{1}{3}K = 1 \tag{5.10}$$

[1] In these plots, a specific time t does not have a significant importance. Here we let time evolve enough so that it can reach asymptotic state if it is possible in that model.

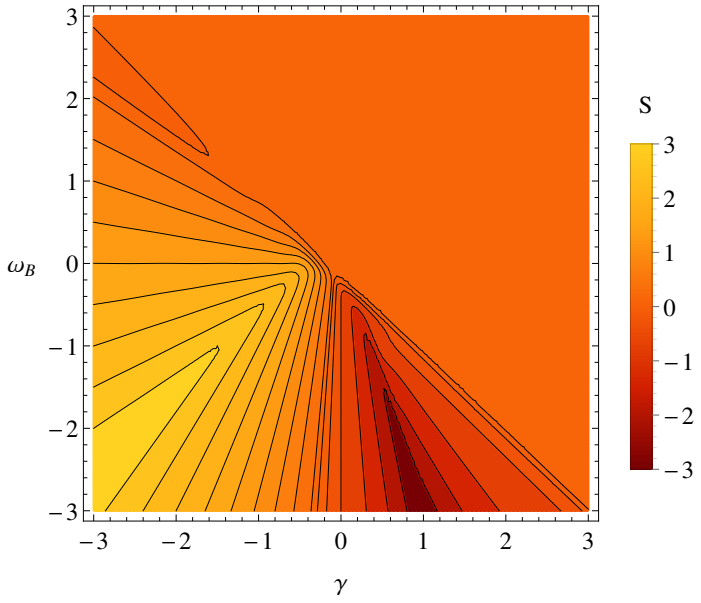

Figure 5.8 Contour plot of shear S according to ω_{B} and γ in a curved universe. It represents the asymptotic state of shear in the universe starting from a matter-dominated state. The axes are γ and ω_{B}, respectively. The contour represents the value of shear S.

which yields [2]

$$\Omega_{\mathrm{S}} \equiv \frac{1}{9}S^2 \quad \text{and} \quad \Omega_{\mathrm{K}} \equiv -\frac{1}{3}K \tag{5.11}$$

In order to avoid confusion, here dark energy density Ω is newly defined as Ω_{M}. These figures show how each density parameters vary as time evolves depending on different dark energy properties in anisotropic curved universe. A matter-dominated flat universe is used as an initial condition.

The plot in case of $\omega = 0, \omega_{\mathrm{B}} = -1$ and $\gamma = -2$ is shown in Fig. 5.9. Roughly shear and dark energy grow and dark matter decays. In detail, curvature parameter decrease gradually but it is relatively very small compared to other parameters. As a consequence, all the density parameters become stable. This model ends up with fairly high quantity of shear property.

The plot in case of $\omega = 0, \omega_{\mathrm{B}} = -1$ and $\gamma = 2/3$ is shown in Fig. 5.10. This case satisfies a shear-free condition. A curvature parameter grows to a high degree with a dark energy parameter. On the other hand, shear does not grow. More specifically a shear term grows, relatively very small though, but it dies out as a curvature term

[2]Note that the sign of newly defined curvature paramter as in relative density parameter form is negative. It can conflict with a formal definition of curvature paramter in Chapter 1. However it is purely derived from our phase variable K and for simplicity makes the sum of all the density parameters be 1.

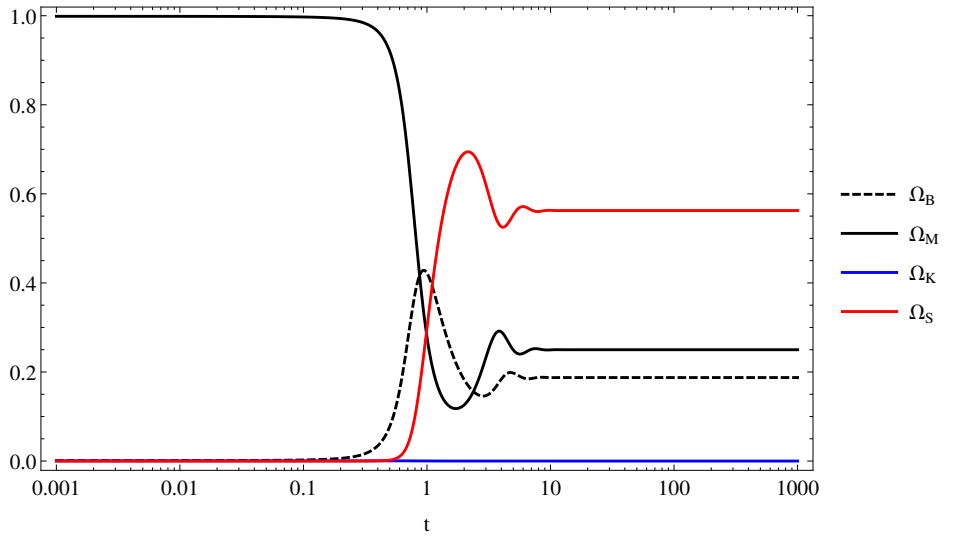

Figure 5.9 Plot of density parameters as a function of time. It is a log-linear plot. This is one of the example case $\omega = 0\,, \omega_B = -1$ and $\gamma = -2$

grows. Dark matter decays as time evolves. This model ends up with fairly high amount of curvature.

Let us take a look at more realistic cosmological models which resemble the universe we live in. Figures 5.11 and 5.12 are in e-folding time scale N which makes today $N = 0$. The evolution of universe model in the case $\omega = 1/3, \omega_B = -1$ and $\gamma = 0.05$ is shown in Fig. 5.11. Hence, here Ω_M actually represents a radiation density parameter. Shear parameter decays as time goes by, therefore this model isotropizes at late times. This figure shows that in this model, a universe is dominated by shear at early times and then is dominated by radiation. Later it goes over to the accelerating stage.

The evolution of universe model in the case $\omega = 0, \omega_B = -1$ and $\gamma = 0.05$ is shown in Fig. 5.12. Here, Ω_M represents a matter density parameter as usual. A shear parameter behaves similarly with Fig. 5.11, however in this model it starts to decay early and then isotropizes. A stage transition from shear to matter and from matter to dark energy is shown clearly. The density parameter values for today correspond to the observations as well. It seems interesing that the future for both cases will reach dark energy domination.

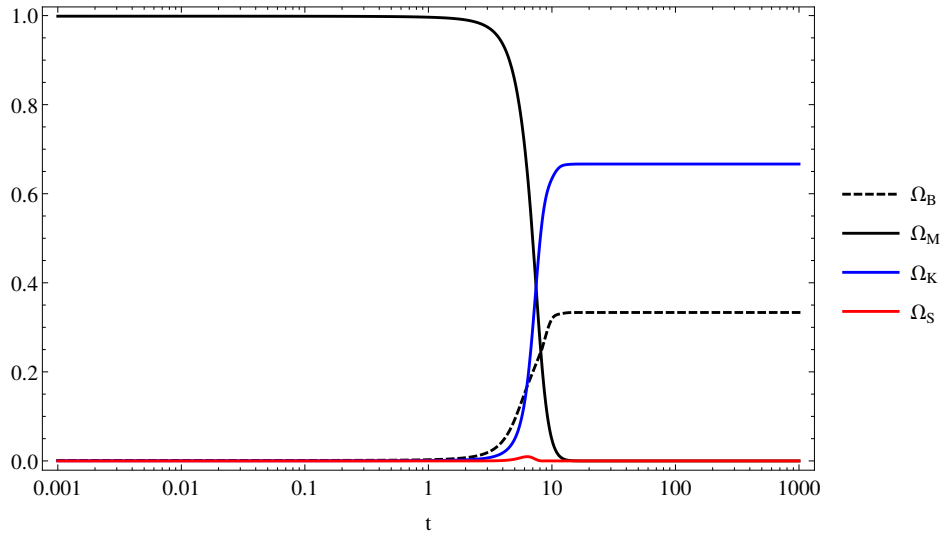

Figure 5.10 Density parameters as a function of time. It is a log-linear plot. This is another example case $\omega = 0\,, \omega_B = -1$ and $\gamma = 2/3$. It is a shear-free condition as well.

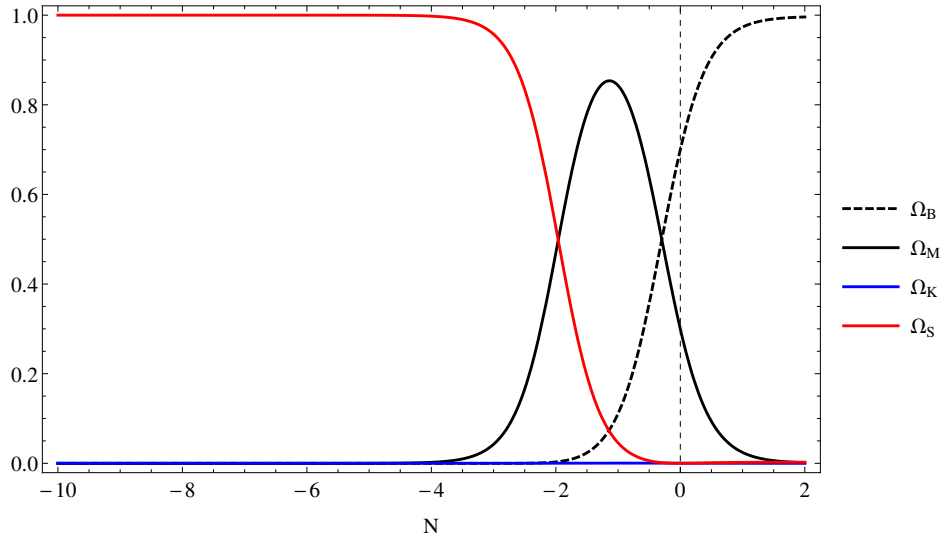

Figure 5.11 Plot of density parameters as a function of e-folding time scale N. This is one of the example case $\omega = 1/3\,, \omega_B = -1$ and $\gamma = 0.05$

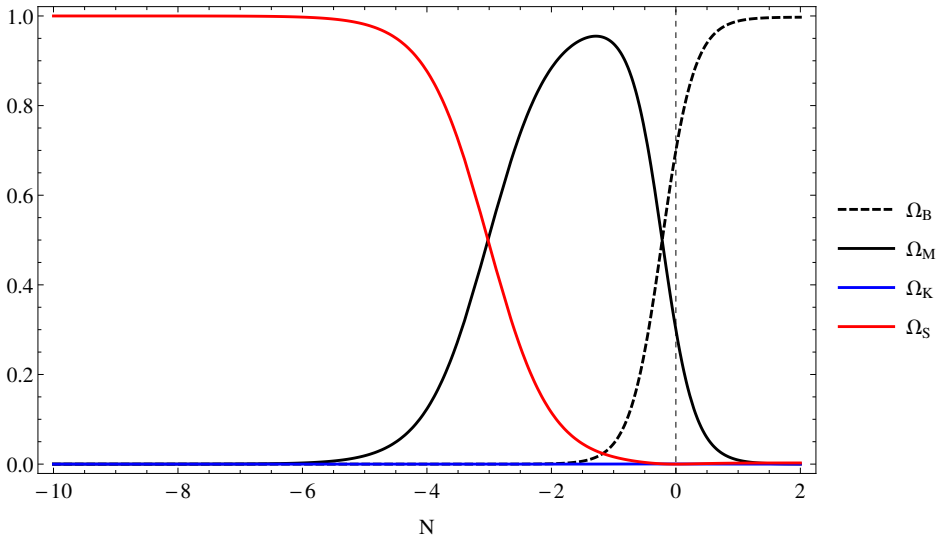

Figure 5.12 Plot of density parameters as a function of e-folding time scale N. This is one of the example case $\omega = 0\,, \omega_{\rm B} = -1$ and $\gamma = 0.05$

Chapter 6

Conclusions

In this work, we studied the possibility that the expansion of the universe in an accelerating rate is caused by an anisotropic equation of state. The motivation of this work comes from the CMB observations which seems to suggest the statistical anisotropy of our universe and the need to test the basic assumptions of cosmology. From the investigation of the anisotropic background dynamics we found that there exists an anisotropic scaling solution for a flat universe and there is no scaling solution for a curved universe.

6.1 Summary and conclusions

We started by parameterization for anisotropic metric which includes three different space-times in their axisymmetric limit. Furthermore we considered a two-fluid system, where only one of the fluids is responsible for possible anisotropic properties. This anisotropic fluid is considered as a background of the system. The equation of state parameter for perfect fluid is defined as ω and for anisotropic fluid ω_{B}. Depending on curvature, the metric is described by the Bianchi I (flat), Bianchi III (negatively curved) and Kantowski-Sachs (positively curved) geometry in terms of the skewness parameter γ. Background dynamical system is constructed in terms of new phase variables, shear S, energy density of perfect fluid Ω, energy density of anisotropic fluid Ω_{B}, and curvature K. Rewriting the Einstein equations in terms of the new phase variables yields the evolution equations for each phase variable with respect to e-folding time scale N. The next step is to obtain the fixed points by solving these evolution equations. The stability of the fixed points was checked under the small perturbations around the fixed point for a flat universe and curved universe separately. In particular, for a curved geometry, the stability of the shear-free condition is checked. The generic asymptotic evolution of the universe

in a simple case is obtained as well. A scaling solution was found both within the matter dominated epoch as well as during an accelerated expansion phase in a flat universe. Additionally, a numerical solution was found which agrees well with the analytical solutions.

The results of this work is summarized in Table 6.1 and 6.2.

Solution	Ω	Ω_{B}	S
FLRW	1	0	0
Empty	0	0	± 3
DE I	0	$\frac{(\omega_{\mathrm{B}}-\gamma-1)(\omega_{\mathrm{B}}+3\gamma-1)}{(\omega_{\mathrm{B}}+\gamma-1)^2}$	$\frac{6\gamma}{\omega_{\mathrm{B}}+\gamma-1}$
DE II	0	$-\frac{\omega_{\mathrm{B}}+\gamma}{4\gamma^2}$	$\frac{3(\omega_{\mathrm{B}}+\gamma)}{2\gamma}$
Scaling	$\frac{3\gamma^2+\gamma(1+\omega-2\omega_{\mathrm{B}})+(\omega-\omega_{\mathrm{B}})(\omega_{\mathrm{B}}-1)}{4\gamma^2}$	$\frac{(1-\omega)(\omega-\omega_{\mathrm{B}}-\gamma)}{4\gamma^2}$	$\frac{3(\omega_{\mathrm{B}}-\omega+\gamma)}{2\gamma}$

Table 6.1 Fixed points in a flat geometry in the limit of axisymmetry in terms of equations of state ω, ω_{B} and skewness paramter γ. Depending on the evolution of expansion of the universe, the names of solutions are the FLRW, Empty, Dark Energy (DE) and Scaling solution. The fixed point corresponds to an anisotropic expansion unless $S = 0$.

Solution	Ω	Ω_{B}	S	K
Empty	0	0	$\frac{3}{2}$	$-\frac{9}{4}$
Matter	-3ω	0	$\frac{3}{2}(1+3\omega)$	$\frac{9}{4}(\omega-1)(3\omega+1)$
DE	0	$-\frac{3\omega_{\mathrm{B}}}{(1+3\gamma)^2}$	$\frac{3(1+3\gamma+3\omega_{\mathrm{B}})}{2(1+3\gamma)}$	$\frac{9(3\omega_{\mathrm{B}}^2+2\omega_{\mathrm{B}}(3\gamma-1)-(1+3\gamma)^2)}{4(1+3\gamma)^2}$

Table 6.2 Fixed points in a curved geometry in the limit of axisymmetry in terms of equations of state ω, ω_{B} and skewness paramter γ. Depending on the evolution of expansion of the universe, the names of solutions are the Empty, Matter, Dark Energy (DE) solution.

6.2 Outlook

This work is done in phenomenological and theoretical aspects. An approach in aspect of cosmological observations would help to understand it better. In particular, explicit constraints can be derived from the amplitude of the quadrupole anisotropy in the CMB. Moreover, the luminosity distance-redshift relationship of the supernovae of type Ia can be used to constrain it. Therefore, within the bounds

from observational data, the anisotropy can be beneficial as a potential explanation of various anomalies in the CMB at the largest angles. What's more, the possibility of an anisotropic generalization of the cosmological constant and inhomogeneous cosmology of anisotropic model for a curved geometry can be studied as well.

Bibliography

Ackerman, L.; Carroll, S. M., and Wise, M. B. Imprints of a primordial preferred direction on the microwave background. *Phys. Rev. D*, 75(8):083502, April 2007. doi: 10.1103/PhysRevD.75.083502.

Akofor, E.; Balachandran, A. P.; Jo, S. G.; Joseph, A., and Qureshi, B. A. Direction-dependent CMB power spectrum and statistical anisotropy from noncommutative geometry. *Journal of High Energy Physics*, 5:092, May 2008. doi: 10.1088/1126-6708/2008/05/092.

Alexander, S. H. S. Is cosmic parity violation responsible for the anomalies in the WMAP data? *Physics Letters B*, 660:444–448, March 2008. doi: 10.1016/j.physletb.2007.12.010.

Armendáriz-Picón, C. Could dark energy be vector-like? *J. Cosmology Astropart. Phys.*, 7:007, July 2004. doi: 10.1088/1475-7516/2004/07/007.

Armendáriz-Picón, C. Footprints of statistical anisotropies. *J. Cosmology Astropart. Phys.*, 3:002, March 2006. doi: 10.1088/1475-7516/2006/03/002.

Barrow, J. D. Cosmological limits on slightly skew stresses. *Phys. Rev. D*, 55:7451–7460, June 1997. doi: 10.1103/PhysRevD.55.7451.

Barrow, J. D. and Matzner, R. A. The homogeneity and isotropy of the Universe. *MNRAS*, 181:719–727, December 1977.

Belinski, V. and Verdaguer, E. *Gravitational Solitons*. Cambridge Monographs on Mathematical Physics. Cambridge University Press, 2001. ISBN 9780521805865.

Bernui, A.; Villela, T.; Wuensche, C. A.; Leonardi, R., and Ferreira, I. On the cosmic microwave background large-scale angular correlations. *A&A*, 454:409–414, August 2006. doi: 10.1051/0004-6361:20054243.

Blake, C.; Brough, S.; Colless, M.; Contreras, C.; Couch, W.; Croom, S.; Davis, T.; Drinkwater, M. J.; Forster, K.; Gilbank, D.; Gladders, M.; Glazebrook, K.; Jelliffe, B.; Jurek, R. J.; Li, I.-H.; Madore, B.; Martin, D. C.; Pimbblet, K.;

Poole, G. B.; Pracy, M.; Sharp, R.; Wisnioski, E.; Woods, D.; Wyder, T. K., and Yee, H. K. C. The WiggleZ Dark Energy Survey: the growth rate of cosmic structure since redshift z=0.9. *MNRAS*, 415:2876–2891, August 2011. doi: 10.1111/j.1365-2966.2011.18903.x.

Blyth, T.S. and Robertson, E.F. *Basic linear algebra*. Springer Undergraduate Mathematics Series. SPRINGER VERLAG GMBH, 2002. ISBN 9781852336622.

Böhmer, C. G. and Harko, T. Dark energy as a massive vector field. *European Physical Journal C*, 50:423–429, April 2007. doi: 10.1140/epjc/s10052-007-0210-1.

Capozziello, S.; Cardone, V. F.; Elizalde, E.; Nojiri, S., and Odintsov, S. D. Observational constraints on dark energy with generalized equations of state. *Phys. Rev. D*, 73:043512, Feb 2006. doi: 10.1103/PhysRevD.73.043512. URL `http://link.aps.org/doi/10.1103/PhysRevD.73.043512`.

Carroll, S. M.; Hoffman, M., and Trodden, M. Can the dark energy equation-of-state parameter w be less than -1? *Phys. Rev. D*, 68(2):023509, July 2003. doi: 10.1103/PhysRevD.68.023509.

Carroll, S.M. *Spacetime and geometry: an introduction to general relativity*. Addison-Wesley Longman, Incorporated, 2004. ISBN 9780805387322.

Clifton, T.; Mota, D. F., and Barrow, J. D. Inhomogeneous gravity. *MNRAS*, 358:601–613, April 2005. doi: 10.1111/j.1365-2966.2005.08831.x.

Copi, C. J.; Huterer, D.; Schwarz, D. J., and Starkman, G. D. On the large-angle anomalies of the microwave sky. *MNRAS*, 367:79–102, March 2006. doi: 10.1111/j.1365-2966.2005.09980.x.

Copi, C. J.; Huterer, D.; Schwarz, D. J., and Starkman, G. D. Large-Angle Anomalies in the CMB. *Advances in Astronomy*, art. 847541, 2010. doi: 10.1155/2010/847541.

Dalal, N.; Abazajian, K.; Jenkins, E., and Manohar, A. V. Testing the Cosmic Coincidence Problem and the Nature of Dark Energy. *Physical Review Letters*, 87(14):141302, October 2001. doi: 10.1103/PhysRevLett.87.141302.

Dodelson, S. *Modern cosmology*. Academic Press. Academic Press, Incorporated, 2003. ISBN 9780122191411.

Ellis, G. F. R. The Bianchi models: Then and now. *General Relativity and Gravitation*, 38:1003–1015, June 2006. doi: 10.1007/s10714-006-0283-4.

Ellis, G. F. R. and van Elst, H. Cosmological Models (Cargèse lectures 1998). In Lachièze-Rey, M., editor, *NATO ASIC Proc. 541: Theoretical and Observational Cosmology*, pages 1–116, 1999.

Eriksen, H. K.; Hansen, F. K.; Banday, A. J.; Górski, K. M., and Lilje, P. B. Asymmetries in the Cosmic Microwave Background Anisotropy Field. *ApJ*, 605:14–20, April 2004. doi: 10.1086/382267.

Freedman, R. and Kaufmann, W. J. *Universe, 6th edition*. 2002.

Gordon, C.; Hu, W.; Huterer, D., and Crawford, T. Spontaneous isotropy breaking: A mechanism for CMB multipole alignments. *Phys. Rev. D*, 72(10):103002, November 2005. doi: 10.1103/PhysRevD.72.103002.

Graham, D. and McRuer, D.T. *Analysis of nonlinear control systems*. Wiley, 1961.

Gumrukcuoglu, A. E.; Contaldi, C. R., and Peloso, M. CMB Anomalies from Relic Anisotropy. *ArXiv Astrophysics e-prints*, August 2006.

Hawking, S.W. and Ellis, G.F.R. *The Large Scale Structure of Space-Time*. Cambridge Monographs on Mathematical Physics. Cambridge University Press, 1973. ISBN 9780521099066.

Hinshaw, G.; Nolta, M. R.; Bennett, C. L.; Bean, R.; Doré, O.; Greason, M. R.; Halpern, M.; Hill, R. S.; Jarosik, N.; Kogut, A.; Komatsu, E.; Limon, M.; Odegard, N.; Meyer, S. S.; Page, L.; Peiris, H. V.; Spergel, D. N.; Tucker, G. S.; Verde, L.; Weiland, J. L.; Wollack, E., and Wright, E. L. Three-Year Wilkinson Microwave Anisotropy Probe (WMAP) Observations: Temperature Analysis. *ApJS*, 170:288–334, June 2007. doi: 10.1086/513698.

Hinshaw, G.; Larson, D.; Komatsu, E.; Spergel, D. N.; Bennett, C. L.; Dunkley, J.; Nolta, M. R.; Halpern, M.; Hill, R. S.; Odegard, N.; Page, L.; Smith, K. M.; Weiland, J. L.; Gold, B.; Jarosik, N.; Kogut, A.; Limon, M.; Meyer, S. S.; Tucker, G. S.; Wollack, E., and Wright, E. L. Nine-Year Wilkinson Microwave Anisotropy Probe (WMAP) Observations: Cosmological Parameter Results. *ArXiv e-prints*, December 2012.

Ishak, M.; Richardson, J.; Garred, D.; Whittington, D.; Nwankwo, A., and Sussman, R. Dark energy or apparent acceleration due to a relativistic cosmological model more complex than the Friedmann-Lemaitre-Robertson-Walker model? *Phys. Rev. D*, 78(12):123531, December 2008. doi: 10.1103/PhysRevD.78.123531.

Jacobs, K. C. Spatially Homogeneous and Euclidean Cosmological Models with Shear. *ApJ*, 153:661, August 1968. doi: 10.1086/149694.

Koivisto, T. Growth of perturbations in dark matter coupled with quintessence. *Phys. Rev. D*, 72(4):043516, August 2005. doi: 10.1103/PhysRevD.72.043516.

Koivisto, T. Matter power spectrum in f(R) gravity. *Phys. Rev. D*, 73(8):083517, April 2006. doi: 10.1103/PhysRevD.73.083517.

Koivisto, T. and Mota, D. F. Dark energy anisotropic stress and large scale structure formation. *Phys. Rev. D*, 73(8):083502, April 2006. doi: 10.1103/PhysRevD.73.083502.

Koivisto, T. and Mota, D. F. Gauss-Bonnet quintessence: Background evolution, large scale structure, and cosmological constraints. *Phys. Rev. D*, 75(2):023518, January 2007. doi: 10.1103/PhysRevD.75.023518.

Koivisto, T. and Mota, D. F. Accelerating Cosmologies with an Anisotropic Equation of State. *ApJ*, 679:1–5, May 2008. doi: 10.1086/587451.

Koivisto, T. S.; Mota, D. F.; Quartin, M., and Zlosnik, T. G. Possibility of anisotropic curvature in cosmology. *Phys. Rev. D*, 83(2):023509, January 2011. doi: 10.1103/PhysRevD.83.023509.

Komatsu, E.; Smith, K. M.; Dunkley, J.; Bennett, C. L.; Gold, B.; Hinshaw, G.; Jarosik, N.; Larson, D.; Nolta, M. R.; Page, L.; Spergel, D. N.; Halpern, M.; Hill, R. S.; Kogut, A.; Limon, M.; Meyer, S. S.; Odegard, N.; Tucker, G. S.; Weiland, J. L.; Wollack, E., and Wright, E. L. Seven-year Wilkinson Microwave Anisotropy Probe (WMAP) Observations: Cosmological Interpretation. *ApJS*, 192:18, February 2011. doi: 10.1088/0067-0049/192/2/18.

Kusse, B.R. and Westwig, E.A. *Mathematical Physics: Applied Mathematics for Scientists and Engineers*. Physics textbook. Wiley, 2010. ISBN 9783527618149.

Land, K. and Magueijo, J. Examination of Evidence for a Preferred Axis in the Cosmic Radiation Anisotropy. *Physical Review Letters*.

Land, K. and Magueijo, J. The Axis of Evil revisited. *MNRAS*, 378:153–158, June 2007. doi: 10.1111/j.1365-2966.2007.11749.x.

Linder, E. V. The dynamics of quintessence, the quintessence of dynamics. *General Relativity and Gravitation*, 40:329–356, February 2008. doi: 10.1007/s10714-007-0550-z.

Macri, L. M.; Stanek, K. Z.; Bersier, D.; Greenhill, L. J., and Reid, M. J. A New Cepheid Distance to the Maser-Host Galaxy NGC 4258 and Its Implications for the Hubble Constant. *ApJ*, 652:1133–1149, December 2006. doi: 10.1086/508530.

Magueijo, J. and Sorkin, R. D. Occam's razor meets WMAP. *MNRAS*, 377:L39–L43, May 2007. doi: 10.1111/j.1745-3933.2007.00299.x.

Mattsson, T. Dark energy as a mirage. *General Relativity and Gravitation*, 42:567–599, March 2010. doi: 10.1007/s10714-009-0873-z.

Mimoso, J. P. and Crawford, P. Shear-free anisotropic cosmological models. *Classical and Quantum Gravity*, 10:315–326, February 1993. doi: 10.1088/0264-9381/10/2/013.

Misner, C.W.; Thorne, K.S., and Wheeler, J.A. *Gravitation: Charles W. Misner, Kip S. Thorne, John Archibald Wheeler*. Gravitation. W. H. Freeman, 1973. ISBN 9780716703440.

Mota, D. F. and Shaw, D. J. Evading equivalence principle violations, cosmological, and other experimental constraints in scalar field theories with a strong coupling to matter. *Phys. Rev. D*, 75(6):063501, March 2007. doi: 10.1103/PhysRevD.75.063501.

Mota, D. F.; Kristiansen, J. R.; Koivisto, T., and Groeneboom, N. E. Constraining dark energy anisotropic stress. *MNRAS*, 382:793–800, December 2007. doi: 10.1111/j.1365-2966.2007.12413.x.

Partridge, R. B. and Wilkinson, David T. Isotropy and homogeneity of the universe from measurements of the cosmic microwave background. *Phys. Rev. Lett.*, 18: 557–559, Apr 1967. doi: 10.1103/PhysRevLett.18.557. URL `http://link.aps.org/doi/10.1103/PhysRevLett.18.557`.

Peacock, J.A. *Cosmological Physics*. Cambridge Astrophysics Series. Cambridge University Press, 1999. ISBN 9780521422703.

Peebles, P. J. and Ratra, B. The cosmological constant and dark energy. *Reviews of Modern Physics*, 75:559–606, April 2003. doi: 10.1103/RevModPhys.75.559.

Peebles, P.J.E. *The Large-scale Structure of the Universe*. Princeton Series in Physics Series. Princeton University Press, 1980. ISBN 9780691082400.

Planck Collaboration, ; Ade, P. A. R.; Aghanim, N.; Armitage-Caplan, C.; Arnaud, M.; Ashdown, M.; Atrio-Barandela, F.; Aumont, J.; Baccigalupi, C.; Banday, A. J., and et al., . Planck 2013 results. XVI. Cosmological parameters. *ArXiv e-prints*, March 2013.

Rakić, A. and Schwarz, D. J. Correlating anomalies of the microwave sky. *Phys. Rev. D*, 75(10):103002, May 2007. doi: 10.1103/PhysRevD.75.103002.

Schimd, C.; Uzan, J.-P., and Riazuelo, A. Weak lensing in scalar-tensor theories of gravity. *Phys. Rev. D*, 71(8):083512, April 2005. doi: 10.1103/PhysRevD.71.083512.

Schweizer, F.; Burns, C. R.; Madore, B. F.; Mager, V. A.; Phillips, M. M.; Freedman, W. L.; Boldt, L.; Contreras, C.; Folatelli, G.; González, S.; Hamuy, M.; Krzeminski, W.; Morrell, N. I.; Persson, S. E.; Roth, M. R., and Stritzinger, M. D. a New Distance to the Antennae Galaxies (ngc 4038/39) Based on the Type ia Supernova 2007sr. *AJ*, 136:1482–1489, October 2008. doi: 10.1088/0004-6256/136/4/1482.

Suzuki, N.; Rubin, D.; Lidman, C.; Aldering, G.; Amanullah, R.; Barbary, K.; Barrientos, L. F.; Botyanszki, J.; Brodwin, M.; Connolly, N.; Dawson, K. S.; Dey,

A.; Doi, M.; Donahue, M.; Deustua, S.; Eisenhardt, P.; Ellingson, E.; Faccioli, L.; Fadeyev, V.; Fakhouri, H. K.; Fruchter, A. S.; Gilbank, D. G.; Gladders, M. D.; Goldhaber, G.; Gonzalez, A. H.; Goobar, A.; Gude, A.; Hattori, T.; Hoekstra, H.; Hsiao, E.; Huang, X.; Ihara, Y.; Jee, M. J.; Johnston, D.; Kashikawa, N.; Koester, B.; Konishi, K.; Kowalski, M.; Linder, E. V.; Lubin, L.; Melbourne, J.; Meyers, J.; Morokuma, T.; Munshi, F.; Mullis, C.; Oda, T.; Panagia, N.; Perlmutter, S.; Postman, M.; Pritchard, T.; Rhodes, J.; Ripoche, P.; Rosati, P.; Schlegel, D. J.; Spadafora, A.; Stanford, S. A.; Stanishev, V.; Stern, D.; Strovink, M.; Takanashi, N.; Tokita, K.; Wagner, M.; Wang, L.; Yasuda, N.; Yee, H. K. C., and Supernova Cosmology Project, T. The Hubble Space Telescope Cluster Supernova Survey. V. Improving the Dark-energy Constraints above z greater than 1 and Building an Early-type-hosted Supernova Sample. *ApJ*, 746: 85, February 2012. doi: 10.1088/0004-637X/746/1/85.

Tsujikawa, S. Modified Gravity Models of Dark Energy. In Wolschin, G., editor, *Lecture Notes in Physics, Berlin Springer Verlag*, volume 800 of *Lecture Notes in Physics, Berlin Springer Verlag*, pages 99–145, March 2010. doi: 10.1007/978-3-642-10598-2_3.

Visser, M. and Barceló, C. Energy Conditions and Their Cosmological Implications. In Cotti, U.; Jeannerot, R.; Senjanovi, G., and Smirnov, A., editors, *COSMO-99, International Workshop on Particle Physics and the Early Universe*, page 98, 2000.